

**The Asian-American variant of human papillomavirus 16 E6  
promotes the Warburg effect and  
hypoxia-inducible factor 1 signalling under hypoxia**

A thesis presented to  
The Faculty of Graduate Studies  
of  
Lakehead University  
by  
SEAN CUNINGHAME

In partial fulfillment of requirements  
for the degree of  
Master of Science in Biology

15 Aug 2014

© Sean Cuninghame, 2014

ProQuest Number: 10611961

All rights reserved

INFORMATION TO ALL USERS

The quality of this reproduction is dependent upon the quality of the copy submitted.

In the unlikely event that the author did not send a complete manuscript and there are missing pages, these will be noted. Also, if material had to be removed, a note will indicate the deletion.



ProQuest 10611961

Published by ProQuest LLC (2017). Copyright of the Dissertation is held by the Author.

All rights reserved.

This work is protected against unauthorized copying under Title 17, United States Code  
Microform Edition © ProQuest LLC.

ProQuest LLC.  
789 East Eisenhower Parkway  
P.O. Box 1346  
Ann Arbor, MI 48106 - 1346

## ABSTRACT

Infection with high-risk human papillomavirus (HPV) is responsible for nearly all cases of cervical cancer, as well as a significant fraction of other ano-genital and head and neck cancers. Specifically, HPV type 16 (HPV16) causes the majority of cervical cancers attributed to HPV infection. Intratypic variation occurs within the HPV16 genome such that naturally occurring variants have been described that display variable risks in promoting cervical cancer. In particular, the Asian-American (AA) variant of HPV16 has been found to be a greater risk factor for the development and earlier onset of invasive cervical cancer than the European Prototype (EP). Keratinocytes transduced with the AA variant were previously shown to have increased levels of glycolytic enzymes, implying AAE6 may enhance the Warburg effect – the tendency of cancer cells to take up higher levels of glucose and metabolize it to lactate. Therefore, glucose consumption and lactate production were assessed in the context of these variants and AAE6 was found to enhance the Warburg effect. To elucidate the mechanism behind this shift in metabolism, the hypoxia-inducible factor 1 (HIF-1) pathway was investigated. HIF-1 is a heterodimeric transcription factor made up of  $\alpha$  and  $\beta$  subunits, and enhances the transcription of genes involved in the Warburg effect. Even under normoxic conditions, HIF-1 $\alpha$  is detectable in AAE6 cells, and its levels are higher in the nucleus than in EPE6 cells. A HIF-1-specific reporter assay found HIF-1 activity to be greater in AAE6 in comparison to EPE6 under hypoxia, a typical hallmark of the tumour microenvironment. Gene expression analysis found that the HIF-1 targets GLUT1 and VEGF-A are induced to a greater degree in AAE6 cells exposed to hypoxia. Future studies can elucidate the functionality of HIF-1 in AAE6's enhanced invasive potential via RNA-interference.

## LAY SUMMARY

Faculty and students in the Department of Biology are bound together by a common interest in explaining the diversity of life, the fit between form and function, and the distribution and abundance of organisms. This particular study sought to understand, on a cellular level, the variation in the cancer-causing potential of two genetic variants of human papillomavirus (HPV) type 16 – a sexually transmitted virus capable of causing cancers of the ano-genital region. The E6 oncogene is one of the major HPV genes responsible for causing cancer. In this study, the E6 gene of the European Prototype and the more aggressive Asian-American HPV16 variant, were investigated with regards to how they affect host cell sugar metabolism and ability to adapt to tumour hypoxia. These interrelated properties are known to influence the ability of cells to progress through the stages of carcinogenesis. The more aggressive HPV16 E6 Asian-American variant exemplified a metabolism conducive to cancer progression, and also adaptive to hypoxia, a condition that arises in many cancers and consequently may promote cancer further. This study furthers our understanding of human papillomavirus biology, while also identifying potential targets for further characterization as therapeutic targets.

## ACKNOWLEDGEMENTS

### *Professional*

I first must extend my sincere gratitude to Dr. Ingeborg Zehbe for taking me on as a graduate student. Under your guidance, I have learned much about not only molecular biology, but also of what it takes to be successful in research. Through my experiences over the past two years, my interest in research has only grown fonder. You have given me the opportunity and freedom to explore my interests and research ideas, and for this I am grateful.

Thank you to my committee members, Drs. David Law and Chris Phenix. By providing your input at meetings regarding experimental design, granting access to laboratory equipment, and offering your encouragement along the way, you have contributed to making my graduate experience an enjoyable one. Thank you to Dr. Sean McKenna for agreeing to be my external thesis reviewer. I value your feedback.

I would be remiss if I did not express my sincere gratitude and appreciation to Dr. Simon Lees and his research assistant, Sarah Niccoli for help with my glucose uptake and hypoxic assays. Not only for access to reagents and equipment, but also for helpful insight into the careful design and execution of these experiments.

Last but not least, thank you to all the students, scientists, and support staff at the Thunder Bay Regional Research Institute. In particular, thank you to Carmen Dorè for your ordering and administrative help. Thank you to fellow lab members, Melissa Togtema and Robert Jackson for their mentorship and guidance throughout my time in the Zehbe lab. Melissa, for taking the time to train me in the wonderful world of cell culture when I first started at the lab, and also for looking after me and the rest of the lab

by being such a wonderful friend, colleague, and lab manager. To Rob, for your continued help in experimental design, data interpretation, and the many hours I'm sure you have spent reading over and editing various bits of my writing. It has truly been a joy to work with you both and I would not have made it to this point if it were not for the two of you.

### ***Personal***

I am lucky to have friends & family who have been extremely supportive prior to, and during, my time in graduate studies. Without your support, none of my accomplishments – academic or extracurricular – would be possible. First and foremost, thank you to Ms. Jazmin Nicholetts for your unwavering support, understanding, and patience. You have always been encouraging, even under the most stressful of times. Also, a big 'Thank You' to Uncle Mark & Auntie Joy for your help over the last few years with every aspect of life outside the lab. Oh, and for all the delicious deserts and meals dropped off to the lab – I'm sure my lab mates appreciate it too! To Wilder & Ian for always being supportive of my schooling. To all the friends I have had the good fortune of making by being a student at TBRRI – particularly Rob, Melissa, Jess, Dave, and Greg for always making coming to the lab enjoyable. Lastly, to all of my friends outside of the lab who provided an always-essential means to relieving some stress whether it by a few good games of FIFA, a round of golf, or a trip to the outdoor rinks. You have all made things a little bit easier when the going got tough, which is greatly appreciated!

## TABLE OF CONTENTS

ABSTRACT.....	i
LAY SUMMARY.....	ii
ACKNOWLEDGEMENTS.....	iii
LIST OF TABLES.....	ix
LIST OF FIGURES.....	x
LIST OF ABBREVIATIONS.....	xii
1 INTRODUCTION.....	1
1.1 Human Papillomaviruses and Cancer.....	1
1.2 Tumour metabolism.....	3
1.3 HIF-1 as a regulator of tumour metabolism.....	8
1.4 Research Rationale.....	10
1.5 Hypotheses.....	12
1.6 Research Aims.....	12
2 MATERIALS AND METHODS.....	14
2.1 Cell Culture.....	14
2.1.1 Cell lines and routine maintenance.....	14
2.1.2 Cryogenic cell storage.....	15
2.1.3 Removal of cells from cryogenic storage for culture.....	16
2.2 E6 DNA Sequencing.....	16
2.2.1 DNA extraction.....	16
2.2.2 Polymerase Chain Reaction (PCR).....	17

2.2.3 Agarose Gel Electrophoresis.....	17
2.2.4 PCR purification .....	18
2.2.5 E6 Sequencing .....	18
2.3 Metabolic profiling .....	19
2.3.1 Glucose uptake assay .....	19
2.3.2 Lactate production assay .....	20
2.4 Protein detection .....	21
2.4.1 Protein extraction.....	21
2.4.2 Gel preparation.....	23
2.4.3 SDS-PAGE .....	23
2.4.4 Western Blot .....	24
2.5 Luciferase Assay.....	25
2.5.1 Transfection efficiency .....	26
2.6.2 Luciferase reporter assay for HIF-1 activity .....	26
2.6 Gene expression analysis .....	28
2.6.1 Sample preparation, RNA Extraction and Quality assessments .....	28
2.6.2 Conversion of RNA to cDNA.....	30
2.6.3 Real-Time Polymerase Chain Reaction .....	30
2.7 Statistical Analysis.....	31
3 RESULTS .....	33
3.1 Characterization of E6 variants used in this study.....	33
3.1.1 Confirmation of variant specific SNPs .....	33
3.1.2 Relative E6 expression is equal between variants of each donor .....	33

3.2 Metabolic phenotype of cells transduced with E6 variants .....	36
3.2.1 Keratinocytes immortalized by AAE6 enhance glucose consumption in comparison to that of EPE6 .....	36
3.2.2 Lactate production is increased by keratinocytes immortalized by AAE6 in comparison to EPE6.....	37
3.3 AAE6-transduced PHFKs increase HIF-1 $\alpha$ protein levels.....	40
3.3.1 Whole cell lysates show HIF-1 $\alpha$ is enhanced in AAE6-transduced keratinocytes .....	40
3.3.2 The nuclear pool of HIF-1 $\alpha$ is enriched by AAE6 in comparison to EPE6 ....	41
3.4 Luciferase reporter assay for HIF-1 reveals HIF-1 transcriptional activity is enhanced under hypoxia in AAE6-transduced keratinocytes. ....	43
3.4.1 GFP transfection optimization .....	45
3.4.2 HIF-1 activity is enhanced under hypoxia in AAE6-transduced keratinocytes in comparison to EPE6-transduced keratinocytes.....	45
3.5 Transactivation of HIF-1 target genes in variant transduced keratinocytes .....	48
4 DISCUSSION .....	56
4.1 The AAE6 variant of HPV16 enhances the Warburg effect in transduced keratinocytes .....	56
4.2 Enhanced levels of HIF-1 $\alpha$ in AAE6-transduced keratinocytes.....	57
4.3 Hypoxia as a requirement to enhance HIF-1 activity in AAE6 transduced keratinocytes .....	59
5 CONCLUSIONS AND FUTURE DIRECTIONS .....	63
6 REFERENCES .....	65

7 APPENDIX..... 75

## LIST OF TABLES

Table 1. TaqMan® (LifeTech) Gene Expression Assays.....	28
Table 2. Detected SNPs in EPE6 and AAE6 from Donor One .....	33

## LIST OF FIGURES

Figure 1. The organization of the human papillomavirus type 16 genome .....	2
Figure 2. Infection by HPV and progression to invasive cancer .....	4
Figure 3. The Warburg Effect.....	6
Figure 4. Reactions catalyzed by firefly and <i>Renilla</i> luciferase .....	31
Figure 5. E6 expression was similar between variants from each donor.....	34
Figure 6. Lactate production of keratinocytes transduced with E6 variants.....	37
Figure 7. Glucose Consumption of keratinocytes transduced with E6 variants .....	38
Figure 8. Western blot analysis of HIF-1 $\alpha$ protein levels in keratinocytes .....	41
Figure 9. Western blot analysis of subcellular fractions of HIF-1 $\alpha$ .....	43
Figure 10. Confirmation of Cignal <sup>TM</sup> reporter plasmid transfection .....	46
Figure 11. AAE6 induces HRE Luciferase activity to a greater degree under hypoxia .	47
Figure 12. Relative GLUT1 mRNA levels in E6-transduced keratinocytes under normoxic and hypoxic conditions.....	50
Figure 13. Relative HK2 mRNA levels E6-transduced keratinocytes under normoxic and hypoxic conditions .....	51
Figure 14. Relative LDHA mRNA levels in E6-transduced keratinocytes under normoxic and hypoxic conditions .....	52
Figure 15. Relative PDK1 mRNA levels in E6-transduced keratinocytes under normoxic and hypoxic conditions. ....	54
Figure 16. Relative VEGF-A mRNA levels expression in E6-transduced keratinocytes under normoxic and hypoxic conditions.....	55
Figure A1. Sequence alignment of EPE6 with HPV16 reference sequence.....	74

Figure A2. Sequence alignment of AAE6 with HPV16 reference sequence..... 75

## LIST OF ABBREVIATIONS

2-NBDG	(2-( <i>N</i> -(7-Nitrobenz-2-oxa-1,3-diazol-4-yl)Amino)-2-Deoxyglucose)
AAE6	Asian-American E6 oncogene
ATP	Adenosine Triphosphate
C-TAD	C-terminal Transactivation Domain (of HIF-1 $\alpha$ )
CAIX	Carbonic Anhydrase IX
CBP	cAMP response-element binding protein Binding Protein
DMSO	Dimethyl Sulfoxide
DPBS	Dulbecco's Phosphate Buffered Saline
eIF-4E	elongation Initiation factor-4E
FIH-1	Factor Inhibiting Hypoxia-Inducible Factor 1
GAPDH	Glyceraldehyde-3-phosphate dehydrogenase
GFP	Green Fluorescent Protein
GLUT1	Glucose Transporter, isozyme 1
HIF-1 $\alpha/\beta$	Hypoxia-inducible Factor 1 alpha/beta subunits
HK2	Hexokinase, isozyme 2
HPRT1	Hypoxanthine phosphoribosyltransferase 1
HPV	Human Papillomavirus
HRE	Hypoxia Response Element
KGM	Keratinocyte Growth Medium
LCR/URR	Long Control Region, also known as Upper Regulatory Region
LDHA	Lactate Dehydrogenase A

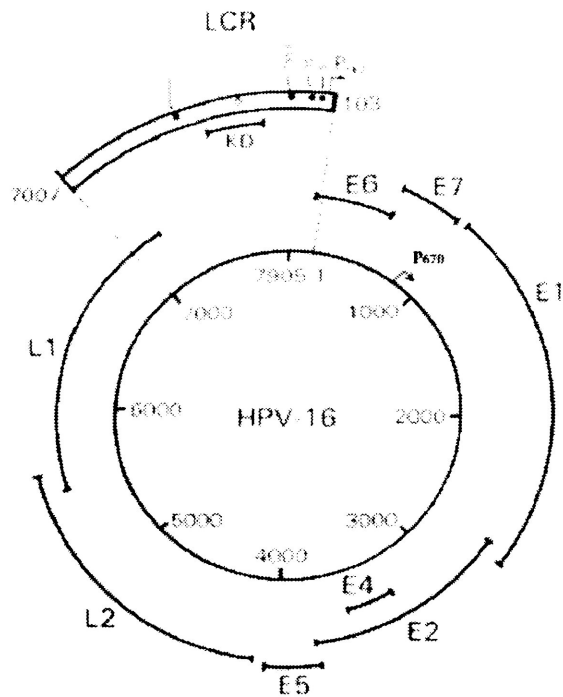
MAPK	Mitogen-activated protein kinase
NADH	Nicotinamide adenine dinucleotide
N-TAD	N-terminal Transactivation Domain (of HIF-1 $\alpha$ )
NLS	Nuclear Localization Signal
ORF	Open Reading Frame
OXPHOS	Oxidative Phosphorylation
PDK1	Pyruvate Dehydrogenase Kinase, isozyme 1
PKM1/2	Pyruvate Kinase, Muscle Isoform 1/2
PHFK	Primary Human Foreskin Keratinocytes
PMSF	Phenylmethylsulfonyl fluoride
PHD-1, 2, 3	Prolyl Hydroxylases, isoforms 1, 2 & 3
PI3K	Phosphoinositol-3-Kinase, referring to the pathway
RTK	Receptor Tyrosine Kinase
STAT-3	Signal Transducer and Activator of Transcription 3
TBS(T)	Tris-Buffered Saline (Tween-20 detergent)
VEGF	Vascular Endothelial Growth Factor A
VHL	von Hippel Lindau (tumour suppressor protein)
WCL	Whole Cell Lysate

# 1 INTRODUCTION

## 1.1 Human Papillomaviruses and Cancer

Approximately 16% of yearly cancer diagnoses worldwide are attributable to an infectious agent, the majority of which are the result of a viral infection (de Martel et al., 2012). One of the most well established links between a viral infection and cancer is that of the human papillomaviruses (HPVs), which cause cancers of the ano-genital region and oral mucosa. Notably, it is estimated that infection with HPV is responsible for up to 99.7% of cervical cancer cases – the second most common type of cancer among women worldwide (Walboomers et al., 1999). While over 170 types of HPVs have been identified, only a small fraction are associated with persistent infection leading to cervical cancer, and thus termed “high-risk” to differentiate them from the “low-risk” types that cause benign warts. Furthermore, of the cervical cancer cases that result from HPV infection, more than half (approximately 55%) result from infection with HPV type 16 (HPV16) (Crow et al., 2012).

The human papillomaviruses are double stranded DNA viruses with a genome that is approximately eight kilobases in length. It contains eight open reading frames (ORFs) under transcriptional regulation of a long control region or upper regulatory region (LCR/URR) (Figure 1). The LCR contains transcription factor binding sites for both viral and endogenous host transcription factors. The genome contains six genes expressed early in the viral life cycle (“E” genes) that are responsible for viral replication, and two late (“L”) genes that code for the viral capsid. The HPV viral life cycle entails virions gaining entry to basal keratinocytes, typically through microscopic abrasions in the epithelium. At this point, the viral capsid is digested and the early genes of the virus



- Function of viral proteins**
- E1:** viral replication
  - E2:** viral replication and transcription
  - E4:** destabilization of cyokeratin network
  - E5:** mediates mitogenic signal of growth factors
  - E6:** major oncoprotein
  - E7:** major oncoprotein
  - L1:** major viral coat protein
  - L2:** minor viral coat protein

**Figure 1. The organization of the human papillomavirus type 16 genome.** The LCR has binding sites for host cell transcription factors as well as viral proteins E1 and E2 that control viral replication and gene expression. P<sub>97</sub>, Early promoter; P<sub>670</sub>, Late promoter. Adapted with publisher permission from Ghittoni et al., 2010.

are expressed (Figure 2) (Doorbar et al., 2012). As basal keratinocytes divide, they give rise to daughter cells that move outward toward the epithelial surface. Once cells reach the surface of the epithelium, they express the L2 and L1 proteins, and subsequent packaging and release of new virions into the surrounding environment occurs (Doorbar et al., 2012).

The two major viral genes that act to induce malignancy in infected cells are the E6 and E7 oncogenes. To date, many cellular functions of these two oncogenes have been elucidated. The E7 gene of high-risk HPV types effectively binds to and deactivates the retinoblastoma tumour suppressor (pRb) protein. The binding of E7 to pRb releases the transcription factors of the E2F family that, in turn, push the cell into the S phase of the cell cycle, thus promoting cell proliferation (Ghittoni et al., 2010). The E6 gene of high-risk HPV causes the breakdown of the tumour suppressor protein, p53, which normally has several anti-tumour effects such as promoting apoptosis and cell cycle arrest (Hock & Vousden, 2012). High-risk E6 has several other functions in immortalization (i.e., extending cellular lifespan) and cellular transformation (to obtain a malignant phenotype) including enhancing telomerase activity (Klingelutz, et al., 1996), as well as enhancing cell proliferation and adhesion (Doorbar et al., 2012).

## **1.2 Tumour metabolism**

Termed the Warburg effect after German physiologist Otto Warburg, it has been well documented that cancer cells take up large amounts of glucose and convert much of it into lactate, as opposed to channeling pyruvate derived from glycolysis into the

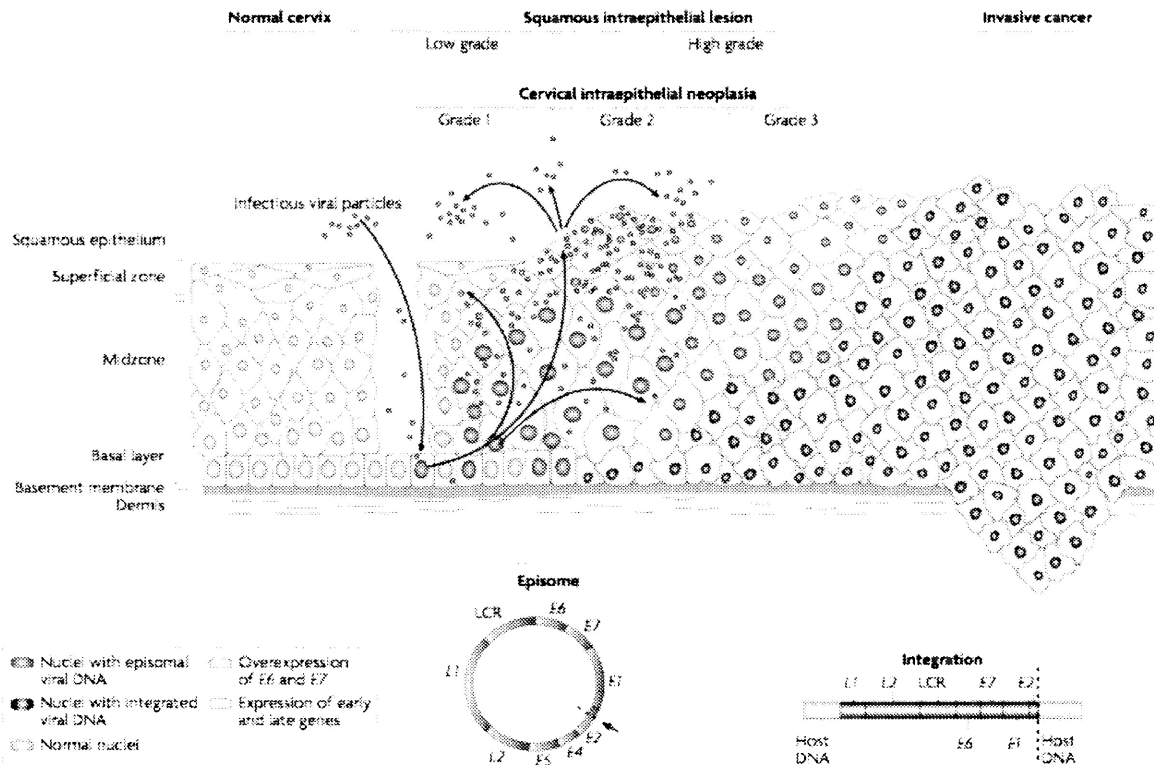


**Figure 2. Infection by HPV and progression to invasive cancer.** HPV virions infect rapidly dividing basal keratinocytes of the epithelium, upon which early genes are expressed and viral DNA is maintained episomally. As infected cells begin to move toward the superficial epithelium with altered differentiation, late genes begin to be expressed and viral packaging occurs. Over the course of several years, if the infection is not cleared by the host immune system, invasive cervical cancer may develop along with integration of the HPV genome into host DNA. Adapted with publisher permission from Woodman et al., 2007.

mitochondria for oxidative phosphorylation (OXPHOS; Figure 3; Vander Heiden et al., 2009). This metabolic shift is reminiscent of cells that are under hypoxic stress. In normal, well oxygenated and differentiated cells, glucose is metabolized to pyruvate, followed by oxidative phosphorylation in order to maximize adenosine triphosphate (ATP) production. Under hypoxic conditions, however, where molecular oxygen is not available as a final electron acceptor, pyruvate is not converted to acetyl-CoA and subsequent oxidative phosphorylation does not occur.

The advantage bestowed to cancer cells by switching their mode of metabolism from one where energy output is maximized, to a much less efficient one in terms of energy (ATP) production is still a topic of debate. While it was initially assumed that Warburg's observations of a switch in metabolism of cancer cells from oxidative phosphorylation to aerobic glycolysis to arise from a tumour microenvironment that is often hypoxic, there is evidence that cancer cells continue to exhibit this type of metabolism, even when exposed to sufficient oxygen for oxidative phosphorylation to occur (Figure 3; Kondoh 2008; Vander Heiden et al., 2009). Consequently, it is hypothesized that this shift in metabolism to a less efficient mode of energy production occurs in proliferating cells to facilitate the transport of nutrients in such a manner that promotes cellular proliferation and survival, and not necessarily ATP production (Vander Heiden et al., 2009). Altering metabolism to rely primarily on glycolysis for ATP production confers several benefits for tumour growth. First and foremost, cancer cells can use the increased glucose influx to provide carbon for the biosynthesis of macromolecules (lipids, nucleotides, proteins) required for cellular proliferation (Kroemer & Pouyssegur, 2008). For example, glucose-6-phosphate can be used for the

production of ribose-5-phosphate to be used in nucleotide synthesis via the pentose phosphate pathway, while dihydroxyacetone phosphate produced from the glycolytic intermediate fructose-1,6-biphosphate is used for the biosynthesis of phospholipids (Lopez-Lazaro, 2008). Secondly, alteration of metabolism to aerobic glycolysis favours tumourigenesis by circumventing the formation of reactive oxygen species (ROS; e.g.,  $O_2^-$ ,  $\cdot OH$ ) resulting from oxidative phosphorylation (Kondoh 2008). Oxidative stress induces replicative senescence and apoptosis, so the Warburg effect may select for cells that are resistant to senescence that results from oxidative phosphorylation (Hsu & Sabatini, 2008). Third, the production of lactic acid lowers the pH of the tumour microenvironment. Lactic acidosis favours tumour growth and invasion by inducing death of normal cells that do not have the typical characteristic of cancer cells to be resistant to low pH. This “acid-mediated invasion” also promotes activity and secretion of extracellular matrix remodeling enzymes such as cathepsins and matrix metalloproteases, while also limiting the immune response to cancer growth, and promoting angiogenesis (Gatenby et al., 2006; Parks et al., 2011). Acidification of the tumour microenvironment as a result of lactate production is associated with a poor clinical outcome and increased risk of metastases (reviewed in Hirschhaeuser et al., 2011; Dhup et al., 2012), including those of the uterine cervix (Walenta et al., 2000).

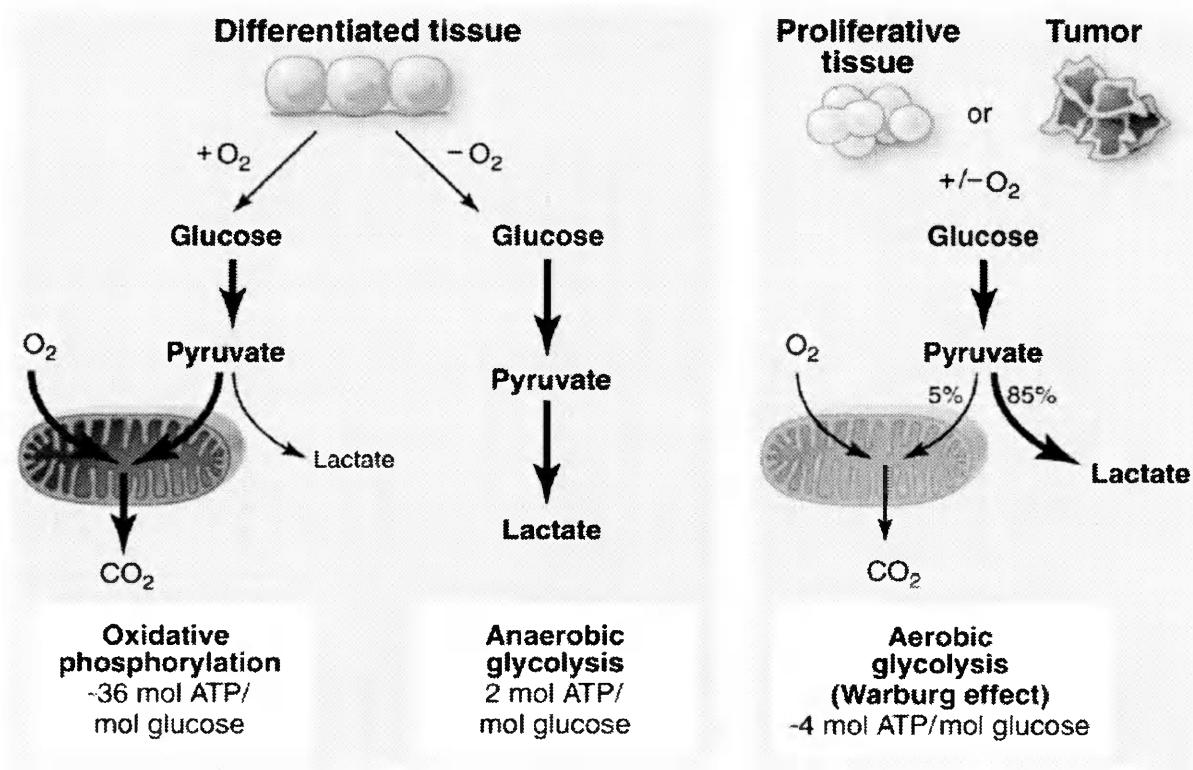


**Figure 3. The Warburg Effect.** Proliferating tissues, regardless of the level of oxygen present, take in glucose and convert much of it to lactate. A large decrease in the amount of ATP produced per molecule of glucose accompanies this change in metabolic fate, which is accommodated for by increasing the influx of glucose. Used with publisher permission from Vander Heiden et al., 2009.

### **1.3 HIF-1 as a regulator of tumour metabolism**

In non-cancerous cells, regulation of anaerobic metabolism relies primarily on the direction of the transcription factor, hypoxia-inducible factor 1 (HIF-1) (DeBarardinis et al., 2008). Transcriptionally active HIF-1 is a heterodimer made up of  $\alpha$ - and  $\beta$ -subunits (the  $\beta$  subunit is also known as aryl hydrocarbon receptor nuclear translocator (ARNT), which also dimerizes with several other transcription factor subunits; Bersten et al., 2013). In most normal, non-hypoxic cells, HIF-1 $\alpha$  is continually synthesized and degraded, while HIF-1 $\beta$  is constitutively expressed to levels that remain relatively constant within the nucleus. HIF-1 activity (the ability to induce transcription of genes), therefore, is largely dependent on the regulation of its  $\alpha$  subunit at several levels including transcription, translation, ubiquitin-mediated protein breakdown, nuclear translocation, and association with transcriptional co-activators.

HIF-1 $\alpha$  mRNA is ubiquitously expressed and its levels are similar for most cell types studied, and remain unaltered between hypoxic and normoxic conditions (Wenger et al., 1997). However, several growth factors and their associated pathways play a role in enhancing HIF-1 $\alpha$  signalling in an oxygen-independent manner by augmenting the translation of HIF-1 $\alpha$  mRNA to protein. Binding of a growth factor (e.g., insulin-like growth factor 1, epidermal growth factor) to its cognate receptor tyrosine kinase (RTK) can lead to activation of the PI3K/Akt or MAPK pathways. Activation of either of these pathways leads to the translation of HIF-1 $\alpha$  mRNA by acting on the translation initiator eIF-4E, stimulating HIF-1 $\alpha$  protein synthesis in an oxygen-independent manner (Agani & Jiang, 2013).

In normoxic cells, HIF-1 $\alpha$  protein degradation is initiated by hydroxylation at one of its proline residues (Pro-402 or Pro-564) by prolyl hydroxylases (PHD-1, PHD-2, and PHD-3) that use molecular oxygen as a co-substrate (Bruick and McKnight, 2001; Semenza, 2001). Upon hydroxylation, HIF-1 $\alpha$ -OH becomes ubiquitinated by the von Hippel Lindau E3 ubiquitin ligase protein (VHL), and subsequent proteasomal breakdown occurs. When there is a lack of oxygen, PHDs become obsolete, resulting in HIF-1 $\alpha$  stabilization and accumulation in the cytoplasm. Once HIF-1 $\alpha$  protein levels increase in the cytoplasm it translocates to the nucleus by way of  $\alpha/\beta$  importins that require a nuclear localization signal (NLS) sequence in HIF-1 $\alpha$ 's N-terminus transactivation domain (N-TAD, Depping et al., 2008). Once in the nucleus, HIF-1 $\alpha$  dimerizes with HIF-1 $\beta$  followed by complexing with the transcriptional co-activators p300/CBP. The formation of the transcription complex is inhibited under hypoxic conditions by the hydroxylase, factor inhibiting HIF-1 (FIH). Similar to the PHDs, FIH hydroxylates the C-terminal transactivation domain (C-TAD) of HIF-1 $\alpha$  at Asn-803, inhibiting the binding of the heterodimer of HIF-1 to its transcriptional co-activator p300 (Lando et al., 2002). If each of these HIF-1-regulatory checkpoints are overcome, active HIF-1 binds to hypoxia response elements (HREs) in target gene promoters, transcriptionally activating a multitude of genes with specific roles in the hypoxic response. To date, over 100 HIF-1 targets have been identified. Although several of the HIF-1 target genes identified thus far are commonly activated in several cell types in response to hypoxia, the specific subset of HIF-1 target genes that are activated under hypoxia can vary between cell type, likely due to the epigenetic effects of other

transcription factors also acting on HIF-1 target genes (Wong et al., 2011, Chi et al., 2006).

Following the identification of HIF-1 as a key hypoxic response regulator, it was found that its overexpression is common in a variety of cancers (Zhong et al., 1999; Krieg et al., 2000). Moreover, increased HIF-1 activity has been associated with an unfavourable prognosis in most cancers, as it activates genes that play a role in promoting the Warburg effect, angiogenesis, cell survival, invasion, and metastasis (Semenza, 2003, 2010, 2012). Originally, this increase of HIF-1 $\alpha$  protein in cancers was primarily attributed to stabilization by environmental hypoxia or genetic mutations (e.g., within VHL) in the pathways leading to the destruction of HIF-1 $\alpha$  (Semenza, 2003). However, it has now become clear that most, if not all, human oncogenic viruses directly enhance HIF-1 signalling, through the various mechanisms affecting its protein levels and activity (Cunningham et al., 2014).

#### **1.4 Research Rationale**

Following the discovery of HPV16 as a causative agent of cervical cancer by Harald zur Hausen in the early 1980's, came several reports that HPV16 E6 and E7 in combination are necessary and sufficient for the immortalization and transformation of primary keratinocytes (Münger et al., 1989, Sedman et al., 1991). However, our laboratory recently found that E6 of HPV16 alone is capable of immortalizing primary keratinocytes (Niccoli et al., 2012). Furthermore, HPV16 E6 variants differ in their ability to immortalize, transform, and migrate keratinocytes *in vitro* (Richard et al., 2010, Niccoli et al., 2012). These HPV16 variants have been named according to the

geographical location in which they were first found: European prototype (EP) and Asian-American (AA); which differ by only three amino acid substitutions based on six single nucleotide polymorphisms (SNPs) in the E6 genetic sequence. While both variants are capable of immortalizing primary keratinocytes, the Asian-American variant E6 (AAE6) is more potent than the European prototype E6 (EPE6) in doing so as suggested by a decreased doubling time (Niccoli et al., 2012). Furthermore, only the AAE6 variant was able to transform keratinocytes to a malignant phenotype *in vitro* and had a greater ability to induce migration of infected cells (Niccoli et al., 2012). These results are in agreement with epidemiological evidence that infection with the AA HPV16 variant is a higher risk factor for high-grade cervical intraepithelial neoplasia and progression to invasive cervical cancer, as well as an earlier onset of malignancy (Zuna et al., 2009, Xi et al., 2007, Berumen et al., 2001). In a three-dimensional organotypic model, AAE6 also has an enhanced ability to drive tumourigenesis (Jackson et al., 2014). However, there still remains a significant knowledge gap in the current understanding of the molecular mechanisms that account for AAE6's superior ability to enhance the immortalization, transformation, and migration in comparison to EPE6, as well as that explaining the epidemiological evidence of AAE6 being a greater risk factor for cervical cancer progression.

Accompanying the reports of AAE6's enhanced immortalization, transformation, and migration ability *in vitro*, is evidence that the Warburg effect and HIF-1 pathway may play a role in these carcinogenic properties. Cells that have AAE6 along with E7 have increased protein levels of metabolic enzymes involved in glycolysis (Richard et al., 2010) as well as carbonic anhydrase IX (CAIX; Niccoli et al., 2012), all of which are

under the regulation of HIF-1 and promote tumourigenesis (Semenza, 2003, Chiche et al., 2009). AAE6-transduced keratinocytes also exhibit lower protein levels of E-cadherin (Niccoli et al., 2012), a key epithelial cell-adhesion protein; the downregulation of which is associated with enhanced migratory ability and can be achieved via HIF-1 transactivating repressors of E-cadherin expression (Onder et al., 2008, Yang et al., 2008, Chen et al., 2008). Thus, the Warburg effect and HIF-1 are potential interrelated pathways that may explain AAE6's increased carcinogenic ability and warrants further investigation.

### **1.5 Hypotheses**

Given the aforementioned evidence for an AAE6-mediated Warburg effect based on alterations in the protein level of metabolic enzymes, as well as several additional effectors of the HIF-1 pathway, it was hypothesized that:

1. H<sub>A</sub>: The HPV16 AAE6 variant induces a greater Warburg effect than EPE6 in keratinocytes transduced with E6 alone, and
2. H<sub>A</sub>: The induction of the Warburg effect is due to the activation of the HIF-1 pathway by the HPV16 AAE6 variant

### **1.6 Research Aims**

To investigate the presented hypotheses, the following approach was used:

1. Quantify the relative amounts of glucose consumed and lactate produced by keratinocytes transduced with the HPV16 E6 oncogene of either the Asian-American or European Prototype variant.

2. Investigate the activation of the HIF-1 pathway in variant-transduced cells:
  - a. Determine the relative levels and subcellular localization of HIF-1 $\alpha$
  - b. Determine the transcriptional activity of HIF-1 under both hypoxic and normal atmospheric oxygen culture conditions.
  - c. Assess gene expression of HIF-1 target genes under both hypoxic and normal atmospheric oxygen culture conditions.

## 2 MATERIALS AND METHODS

### 2.1 Cell Culture

#### 2.1.1 Cell lines and routine maintenance

All cell cultures used in this study were maintained in a 37°C incubator with 5% CO<sub>2</sub>, 95% air. For hypoxia incubation, a hypoxic incubator (Coy Lab Products, Grass Lake, M.I.) was used with a constant oxygen percentage of 1% achieved by nitrogen gas infusion. Media used for each experiment was first equilibrated to 1% O<sub>2</sub> conditions by placing it in a culture vessel with the lid off in the incubator for a minimum of 60 minutes. All experiments carried out on cells exposed to hypoxia were done so after 24 hours of 1% O<sub>2</sub> incubation.

Two donors of Primary Human Foreskin Keratinocytes (PHFKs, cat. #102-05n) were retrovirally transduced with either the EP or AA variant alongside a hemagglutinin (HA) tag on the C-terminus on separate occasions by previous lab members Christina Richard and Sarah Niccoli (Richard et al., 2009, Niccoli et al., 2012). For simplicity, those transduced by CR are denoted as Donor 1 and those of SN, Donor 2. All experiments herein were conducted on cells in passages 70 – 80 (Donor 1) and 37 – 45 (Donor 2).

Untransduced PHFKs served as a HPV16 negative control, and HeLa cells (HPV18+, ATCC, Manassas, VA, cat. # CCL-2) were used as a HIF-1 $\alpha$  positive control in Western blot procedures. Both transduced and untransduced PHFKs were cultured in Serum-Free Keratinocyte Growth Medium (KGM, Cell Applications Inc., San Diego, CA, cat. #131-500) that was changed every other day. HeLa cells were cultured in Dulbecco's Minimum Essential Medium (DMEM, Sigma-Aldrich, St. Louis, MO, cat.

#D5796) supplemented with 10% fetal bovine serum (FBS, Sigma-Aldrich, cat. #F6178) and 1% antibiotics/antimycotics (Invitrogen, Carlsbad, CA, cat. #15240-062) and media was changed every three days. For all cell types, passaging was accomplished via trypsin (Fisher Scientific, Mississauga, ON, cat. #SH3023602) that was subsequently neutralized by Trypsin Neutralizing Solution (Cell Applications Inc., San Diego, CA, cat. #080-100) for HFKs or by supplemented medium for HeLa. HeLa cells were washed with Sterile Phosphate Buffer Saline (DPBS, Invitrogen, cat. #14190) prior to the addition of trypsin to remove residual medium containing FBS.

To begin the following passage, ~300,000 cells were seeded back for HFKs following centrifugation of collected cells to pellet them and remove any residual trypsin and neutralizing solution. A 1:20 dilution factor was used to passage HeLa cells without centrifugation.

### *2.1.2 Cryogenic cell storage*

To ensure a continual supply of cells, vials were prepared during passaging for long-term cryogenic storage. Following trypsin neutralization, cells were spun down and resuspended in their respective growth medium and counted. The desired amounts of cells were then placed in a solution with final volumes of 900  $\mu$ L of growth medium and 100  $\mu$ L of dimethyl sulfoxide (DMSO, Sigma-Aldrich, cat. #34869) in 1.5 mL cryogenic storage vials (Fisher Scientific, cat. #03-337-7Y). Cells were frozen to  $-80^{\circ}\text{C}$  at a controlled rate of  $-1^{\circ}\text{C}/\text{min}$  by placing the tubes in a controlled freezing container (Fisher Scientific, cat. #5100-0001). Cryovials were then transferred to liquid nitrogen for long-term storage.

### *2.1.3 Removal of cells from cryogenic storage for culture*

To commence culture of cells from cryogenic storage, cryotubes were safely removed from liquid nitrogen storage and warmed to room temperature. For HeLa cells, the contents of the tube were centrifuged (Beckman, Mississauga, ON, Model #GS-6KR) at 25 x g to pellet the cells, allowing for the removal of DMSO from the supernatant. For HFKs, the entire 1 mL contents of the tube were added to 10 mL of KGM to dilute DMSO to non-toxic concentrations without the application of centrifugation as per distributor instructions. Growth medium was changed the following day to ensure the removal of residual DMSO.

## **2.2 E6 DNA Sequencing**

### *2.2.1 DNA extraction*

To confirm the retrovirally transduced cells used in this study harboured the proper E6 SNPs, E6 DNA sequencing was performed. Cells were grown to 70 – 80% confluence in a 10 cm tissue culture plate and trypsinized to release the cells. Trypsin neutralizing solution was added and the cells were spun down at 25 x g. The cell pellet was washed with DPBS and spun down a second time before storing at -80°C until all samples were collected. DNA was extracted from cell pellets using the DNeasy® Blood & Tissue Kit (Qiagen, Valencia, CA., cat. #69504) with isolated DNA eluted from a mini spin column in 200 µL of buffer AE. The concentration of DNA was determined using a Synergy 4 plate reader (BioTek, Winooski, VT) with a Take-3 microvolume plate. Pure DNA samples were accepted as having an  $A_{260/280} \geq 1.8$ , indicating low levels of protein contamination.

### 2.2.2 Polymerase Chain Reaction (PCR)

PCR was used to amplify the E6 gene from each sample. The applicable volume for 100 ng of DNA was added to 2.50  $\mu$ L 10X PCR buffer, 1 mM MgCl<sub>2</sub>, 200  $\mu$ M dNTPs, 0.5  $\mu$ M of both an HPV16 E6 forward (5'-CAATGTTTCAGGACCCACA-3') and reverse (5'-GTTTCTCTACGTGTTCTTGA-3') primers, 2 units of Taq Polymerase, and nuclease free (NF)-dH<sub>2</sub>O to bring the final reaction volume to 25  $\mu$ L. A template-free control that contained NF-dH<sub>2</sub>O in lieu of DNA was also ran. The reactions were run with the previously optimized parameters of 40 cycles of 1 minute at 94°C for denaturation, 1 minute at 56°C for annealing and 2 minutes at 72°C for extension. The extension step of cycle 40 was lengthened to 7 minutes and the reaction mixtures were cooled to 4°C.

### 2.2.3 Agarose Gel Electrophoresis

Confirmation of E6 amplification was achieved using agarose gel electrophoresis. A 1.5% agarose gel was poured by mixing 0.9 g agarose into 60 mL of sterile 1X TBE buffer (10.8 g Tris Base, 5.5 g boric acid, 2 mM EDTA). The solution was heated and 3  $\mu$ L of ethidium bromide was added before pouring the gel. The gel was allowed to polymerize for 45 – 60 minutes. A 100 bp DNA ladder (New England Biolabs, Whitby, ON, cat. #N0467) was added to the first lane. A 10  $\mu$ L aliquot of each of the PCR-amplified samples was mixed to 2  $\mu$ L 6X loading dye (Fermentas, Mississauga, ON, cat. #R0611) and loaded into separate wells of the agarose gel. The gel was ran for 1 hour at 100 V and imaged using the BioSpectrum 410 UVP camera and VisionWorks LS software on a UV transilluminator.

#### *2.2.4 PCR purification*

If non-specific bands were observed by agarose gel electrophoresis, PCR products were purified from the agarose gel in order to remove any non-specific bands observed that did not correspond with the 448 bp amplicon of E6. The 448 bp amplicons were cut out of the gel aided by UV transilluminator to observe the bands. The QIAquick Gel Extraction Kit (Qiagen, cat. #28704) was used to extract the DNA from the gel and purify the PCR product by washing and elution from a microcentrifuge column with 30  $\mu$ L of Buffer EB. A second gel was run to confirm elimination of non-specific bands from these samples. In cases where no non-specific bands by agarose gel electrophoresis were found following PCR amplification, the remaining PCR sample was purified using the QIAquick PCR purification Kit (Qiagen, cat. #28104) with elution from a microcentrifuge column 30  $\mu$ L buffer EB. Samples were stored at -20°C.

#### *2.2.5 E6 Sequencing*

To ensure E6 variant DNA had the appropriate SNPs, E6 sequencing was carried out at the Paleo-DNA laboratory at Lakehead University. Purified PCR samples were diluted to 2 ng/ $\mu$ L. A 10  $\mu$ L aliquot of each sample, and each of the forward and reverse E6 primers used in PCR were used for sequencing. Forward and reverse reads were aligned using BioEdit Sequence Alignment Software v7.1.9. The consensus sequence obtained for each sample was matched with the HPV16 E6 reference sequence (Sequence ID: NC\_001526.2) on GenBank to confirm the identity of SNPs for EPE6 and AAE6.

## 2.3 Metabolic profiling

### 2.3.1 Glucose uptake assay

To quantify the rate of glucose uptake, a fluorescently tagged glucose analog, 2-deoxy- 2- [(7-nitro-2,1,3-benzoxadiazol-4-yl)amino]-D-glucose (2-NBDG, Cayman Chemical, cat. #11046) was used. A 100 mM solution of 2-NBDG was prepared by dissolving it in DPBS, and 1  $\mu$ L of this solution was added to 999  $\mu$ L of Krebs-Ringer Phosphate Buffer (KRPH; 140 mM NaCl, 5 mM KCl, 2.5 mM CaCl<sub>2</sub>, 1mM MgSO<sub>4</sub>, 1 mM KH<sub>2</sub>PO<sub>4</sub>, 10 mM HEPES) to make a 100  $\mu$ M 2-NBDG solution which was then added to 80% confluent cells in a 6-well plate. An adjacent control well which did not receive 2-NBDG (only 1 mL of KRPH) served as a negative control in each independent experiment to determine background fluorescence in the cell lysate not due to 2-NBDG uptake.

Cells were incubated with 2-NBDG for 30 minutes at which time the buffer was removed by vacuum and the wells were washed 3 times with 5 mL of DPBS. Cells were then lysed in 150  $\mu$ L of NP40 lysis buffer (1% v/v NP-40, 1% v/v sodium deoxycholate, 40 mM KCl, 20mM Tris-HCl, pH = 7.4). Cells were scraped from the plate, the lysate was collected and then centrifuged at 21,000 x g for 5 minutes at 4°C to pellet the cell debris. From the cell lysate, technical duplicates of 50  $\mu$ L were added to wells of a black-coated 96-well plate and fluorescence was read on a BioTek FL<sub>X</sub>800 Fluorescence microplate reader. Following fluorescence readings, protein amounts were determined using the Bradford Assay method. Bradford assays were performed with a 5  $\mu$ L portion of the extracted protein added to 100  $\mu$ L of Bradford Assay Dye Reagent (BioRad, Mississauga, ON, cat. #500-0006) with 400  $\mu$ L dH<sub>2</sub>O and chilled on ice for 5 minutes.

Following incubation, 300  $\mu$ L of the solution was added to a well of a 96-well plate (Fisher, cat. #087722c) along with standards of known concentrations (1, 2, 3, 5, 7.5, 10, and 20  $\mu$ g/ $\mu$ L) of Bovine Serum Albumin (BSA, Amresco, Solon, OH, cat. #0332-100G) in lysis buffer. Protein concentration was determined using OD measurements at 595 nm of standards and samples on a PowerWave XS spectrophotometer (BioTek, Winooski, VT). The fluorescence of cell lysates not treated with 2-NBDG was subtracted from those that were incubated with 2-NBDG to normalize for the background fluorescence of the cell lysates not attributable to 2-NBDG uptake.

### *2.3.2 Lactate production assay*

Cells were grown to 50% confluence in 6-well plates, at which time the cells were washed three times with 10 mL DPBS and fresh media (10 mL) was given to the cells. The cells were allowed to incubate for 24 hours after which media was removed from the cells and stored momentarily in 15 mL tubes. Cells were washed once with DPBS and cell lysis was performed to obtain protein amounts for normalization. To lyse cells, 150  $\mu$ L of RIPA buffer (50 mM Tris-HCl pH 7.5, 150 mM NaCl, 0.1% SDS, 1% sodium deoxycholate, 1% Triton X-100, 5 mM EDTA, 10 mM NaF) with the fresh addition of 10 mM phenylmethylsulfonyl fluoride (PMSF), a 1:100 dilution of Protease Inhibitor Cocktail (Sigma, cat. #P8340), 12.5  $\mu$ L of activated  $\text{Na}_3\text{VO}_4$  (Sigma, cat. #6508) was added to each plate and incubated on ice for 5 minutes. Cells were scraped and collected into microcentrifuge tubes, vortexed, and incubated on ice for an additional 20 minutes. The lysates were centrifuged in a pre-chilled (4°C) microcentrifuge (Eppendorf, Mississauga, ON, cat. #5414C) at 21,000 x g for 10 minutes to remove cellular debris.

The supernatant of the lysate was collected for protein quantification by Bradford assay as described in Section 2.3.1.

To determine the amount of lactate produced by each cell type, the EnzyChrom L-Lactate Assay kit (BioAssays Systems, Hayward, CA, cat. #ECLC-100) was used which is based on the lactate dehydrogenase (LDH)-mediated oxidation of L-lactate to produce NADH. The NADH produced is then used as a cofactor by a second enzyme, diaphorase to reduce a tetrazolium compound to formazan. This reaction is accompanied by an increase in absorbance at 565 nm, giving an indication of the amount of lactate present in a sample. Standards of varying concentrations (0 – 2.0 mM L-Lactate) were prepared in unconditioned cell culture medium. To an aliquot of a 1:10 dilution of 20  $\mu$ L of media from each sample and standard, 80  $\mu$ L of working reagent was added which contained the manufacturers recommended amount of reagents (60  $\mu$ L of Tris-HCl buffer containing Bovine Serum Albumin (BSA), 1  $\mu$ L of LDH, 1  $\mu$ L diaphorase, 10  $\mu$ L of NAD solution and 14  $\mu$ L MTT solution (thiazolyl blue tetrazolium bromide)). The OD<sub>0</sub> at 565 nm was measured at time zero and again 20 minutes after the addition of the working reagent (OD<sub>20</sub>). The OD<sub>0</sub> for each sample was subtracted from its respective OD<sub>20</sub> and the lactate concentration was determined from the standards.

## **2.4 Protein detection**

### *2.4.1 Protein extraction*

Cells were grown in 10 cm tissue culture plates until they reached 80 – 90% confluence. As a HIF-1 $\alpha$  positive control, HeLa cells were treated overnight with 150  $\mu$ M of the hypoxic mimetic CoCl<sub>2</sub>. Medium was removed from the cells, which were then

washed twice with 5 mL of DPBS and placed on ice. To obtain whole cell lysates (WCLs), 250  $\mu$ L of cold RIPA buffer (50 mM Tris-HCl pH 7.5, 150 mM NaCl, 0.1% SDS, 1% sodium deoxycholate, 1% Triton X-100, 5 mM EDTA, 10 mM NaF) with the fresh addition of 10 mM PMSF, a 1:100 dilution of Protease Inhibitor Cocktail (Sigma, cat. #P8340), 12.5  $\mu$ L of activated  $\text{Na}_3\text{VO}_4$  (Sigma, cat. #6508) was added to each plate and incubated on ice for 5 minutes. Cells were scraped and collected into microcentrifuge tubes, vortexed, and incubated on ice for an additional 20 minutes. The lysates were centrifuged in a pre-chilled (4°C) microcentrifuge (Eppendorf, Mississauga, ON, cat. #5414C) at 21,000 x g for 10 minutes to remove cellular debris. The supernatant of the lysate was collected for protein quantification by Bradford assay as described in Section 4.2.1.

For separation of nuclear and cytoplasmic fractions, the NE-PER™ Nuclear and Cytoplasmic Extraction Kit (ThermoFisher Scientific, Waltham, WA, cat. # 78833) was used. Cells were grown as for whole cell lysates and 200  $\mu$ L of cold CER I buffer was added that contained identical protease inhibitor concentrations as described for whole cell lysates. Cells were scraped and incubated for 10 minutes on ice, at which point 11  $\mu$ L of CER II was added and the lysate was spun down for 5 minutes at 16,000 x g in a pre-chilled (4°C) microcentrifuge. The supernatant that contained the cytoplasmic portion was removed and added to a 0.5 mL microcentrifuge tube and stored on ice until use. The pelleted material that contained the cell nuclei was washed with 0.5 – 1.0 mL PBS to remove any remaining protein from the cytoplasmic portion. The nuclei were then lysed in 60  $\mu$ L of NER with the identical dilution of protease inhibitors as for WCLs. The lysate was allowed to incubate on ice for 40 minutes with grinding approximately every 5

minutes with a plastic tissue grinder and vortexed every 10 minutes. The lysate was spun down for 5 minutes at 16,000 x g in a pre-chilled (4°C) microcentrifuge. Aliquots of 5 µL of each subcellular fraction were used for protein estimation by the Bradford method.

#### *2.4.2 Gel preparation*

To detect relative amounts of proteins of interest in samples, SDS-PAGE followed by Western blotting was performed. SDS-PAGE gels were cast by first preparing a separating gel mixture in dH<sub>2</sub>O containing 375 mM Tris-HCl (pH 8.8), 0.1% sodium dodecyl sulphate (SDS), 0.06% ammonium persulfate (APS, St. Louis, MO, cat. #A9164) and 0.1% TEMED (Sigma St. Louis, MO, cat. #T7024) and 8% acrylamide (Bio-Rad, Hercules, CA, cat. #161-0146). This solution was pipetted between two PAGE glass plates and allowed to polymerize for 15 minutes, after which a stacking gel containing the same components but with 4% acrylamide was added on top of the separating gel and a comb placed in the solution to create the wells in which samples could then be loaded. The stacking gel was allowed to polymerize for at least 30 minutes.

#### *2.4.3 SDS-PAGE*

Using known concentrations determined via Bradford assays, the appropriate amount of protein was added in a 5:1 dilution to 6X SDS loading buffer (375 mM Tris-HCl pH 6.8, 10% SDS, 50% glycerol, 0.03% bromophenol blue) with freshly added dithiothreitol (Fisher, cat. #BP1725) to a final concentration of 600 nM and the total volume of each sample was calculated. 1X SDS was added to samples to bring their volume to that of the highest total volume following 6X SDS, to ensure equal volume

loading for each sample. Samples were then heated for 5 minutes at 70°C (for HIF-1 $\alpha$ ) or 95°C, spun down at 21,000 x g for 1 minute and loaded to the wells of the prepared SDS-PAGE gel that was placed in a 1X Running Buffer solution prepared from adding 100 mL of 10X Running Buffer (30.3 g Tris Base, 144 g glycine, 0.5% SDS in 1 L of dH<sub>2</sub>O) to 900 mL of dH<sub>2</sub>O. After addition of the denatured samples to their respective wells of the gel, the gel was ran at 100V until the dye front passed through the stacking gel, at which point the voltage was increased to 120V and the gel was ran until the dye front reached the bottom of the gel.

#### *2.4.4 Western Blot*

Following the separation of extracted proteins by SDS-PAGE, the gel was placed for 20 minutes in cold 1X Transfer Buffer that was prepared from adding 100 mL of 10X Transfer Buffer (30.3 Tris Base, 144 g glycine in 1 L of dH<sub>2</sub>O) to 900 mL of dH<sub>2</sub>O. A polyvinylidene difluoride (PVDF) membrane was cut to approximately 10 cm x 10 cm and soaked in methanol for 5 minutes, followed by a soak in cold transfer buffer for 20 minutes prior to protein transfer from the gel for 1 hour at 100 V. The membrane was then rinsed briefly in 1x Tris buffered saline with 0.05% Tween-20 that was prepared from adding 100 ml of 10X Tris buffered saline (30.3 g Tris Base, 87.6 g NaCl in 1 L dH<sub>2</sub>O with pH adjusted to 7.5) to 900 mL dH<sub>2</sub>O and adding 500  $\mu$ L of Tween-20 (0.05% TBST). The membrane was subsequently blocked for 1 hour in 5% non-fat milk in 0.05% TBST. When possible, the membrane was cut in order to allow for concurrent primary antibody incubation of several proteins. Primary antibody incubation followed overnight with agitation at 4°C with 5% non-fat milk in 0.05% TBST with HIF-1 $\alpha$  (1:500 dilution,

BD Biosciences, Mississauga, ON, cat. #610958), HIF-1 $\beta$  (1:1000, BD Biosciences, cat. #611078),  $\beta$ -Actin (1:1000, Santa Cruz Biotechnology, Dallas, TX, cat. #sc-1616), Lamin B1 (1:1000, Abcam, Cambridge, MA, cat. #16048),  $\alpha$ -Tubulin (1:8000, Sigma, cat. #T9026). The following day, the membrane was washed 4 x 5 minutes in 0.05% TBST before the addition of secondary antibody at varying dilutions species specific to the primary antibody that was used. Secondary antibody incubation was performed for 1 hour at room temperature in 0.05% TBST with 5% non-fat milk. The membrane was washed again 4 x 5 minutes in 0.05% TBST before developing the membrane with an enhanced chemiluminescence kit (Perkin Elmer Inc., Waltham, MA, cat. #NEL100001EA) by mixing 1 mL of each of the two solutions and adding this solution to the membrane allowed to incubate for 1 minute with agitation. The membrane was imaged with a BioSpectrum 410 UVP camera and VisionWorks LS software using exposure times optimized for the specific protein of interest. Densitometry was performed using the density analysis tool provided with VisionWorks software using  $\beta$ -actin as a loading control for whole cell lysates, lamin B1 for nuclear fractions, and  $\alpha$ -tubulin for cytoplasmic extracts.

## **2.5 Luciferase Assay**

The activity of the HIF-1 transcriptional complex was measured using the commercially available Cignal luciferase assay with firefly and *Renilla* luciferase plasmids mixed in a 40:1 ratio (SABiosciences, Frederick, MD, cat. #CCS-007L). The luciferase plasmid encodes a HIF-1 responsive construct containing tandem repeats of HRE's joined to a TATA promoter of the firefly luciferase assay. The constitutively

expressing *Renilla* construct encodes the *Renilla* luciferase gene under the control of a CMV promoter to act as an internal control for normalizing transfection efficiency.

### 2.5.1 Transfection efficiency

Prior to determining HIF-1 activity in E6-transduced keratinocytes, optimization of the transfection parameters was carried out. A GFP positive control plasmid that constitutively expresses GFP is included with the firefly and *Renilla* plasmids that allows for visual confirmation of transfection by fluorescent microscopy with filters having an excitation of 470 nm and an emission of 515 nm. A qualitative assessment of transfection efficiency was carried out using several transfection reagents including HiPerfect (Qiagen, cat. #301707), FuGene 6 (Promega, Madison, WI., cat. #E2692), Mirus *TransIT*-2020 (Mirus, Madison, WI, cat. #MIR5404), *TransIT*-LT1 (Mirus, cat. #MIR2304, and *TransIT*-X2 (Mirus, cat. #MIR6003). Variable amounts of plasmid and transfection reagent in the recommended ranges for each individual reagent were used to determine the optimal conditions for transfection of the luciferase plasmids.

### 2.6.2 Luciferase reporter assay for HIF-1 activity

Once the optimal parameters for transfection of the firefly and *Renilla* plasmids were determined, analysis of the specific activity of HIF-1 in E6-transduced cells was performed under both normoxic and hypoxic conditions using a reverse transfection method. To prepare transfection complexes, a stock solution was mixed that had sufficient volume for 7 transfections, for 3 technical replications per experiment of both EPE6 and AAE6-transduced cells with an additional transfection volume to account for

pipetting errors. To do this, 341.6  $\mu\text{L}$  of KGM was mixed with 1.4  $\mu\text{L}$  of Mirus *TransIT*-2020 and 7  $\mu\text{L}$  of plasmid mixture. Of this, 50  $\mu\text{L}$  was added to individual wells of a white coated Corning® 96-well clear bottom plate (VWR, Radnor, PA., cat. #29444-010). Cells were trypsinized from T75 flasks when at 80 – 90% confluence and diluted to a concentration of  $4.0 \times 10^5$  cells/mL in KGM. From this, 50  $\mu\text{L}$  of cell suspension was added to wells harbouring 50  $\mu\text{L}$  of the transfection complex to give a final volume of 100  $\mu\text{L}$  and  $2.0 \times 10^4$  cells. Cells were allowed to incubate for 48 hours, at which point 75  $\mu\text{L}$  of fresh KGM was given and the cells incubated either under normoxia or hypoxia for an additional 24 hours.

To measure the amount of firefly or *Renilla* luciferase activity the Dual-Glo® Luciferase Assay System (Promega, cat. #E2920) was used. Upon receipt, the entire contents of the Dual-Glo® Luciferase Buffer was added to the bottle of lyophilized Dual-Glo® Luciferase Substrate to make the Dual-Glo® Luciferase Reagent. The Dual-Glo® Luciferase Reagent contains beetle luciferin, a substrate for recombinant firefly luciferase that is not produced endogenously by mammalian cells and produces light when converted to oxyluciferin (Figure 4A). Thus, the amount of light produced by this reaction gives an indirect measurement of the amount of firefly luciferase produced by HIF-1. Immediately prior to firefly luciferase measurement, the media was removed from the cells and 75  $\mu\text{L}$  DPBS was added to wells because Phenol Red in the media interferes with the luciferase signal. An equal volume of Dual-Glo® Luciferase Reagent to that of the DPBS in the wells (75  $\mu\text{L}$ ) was added with a multichannel pipette and mixed thoroughly by pipetting. The mixture was incubated at room temperature for 15 minutes, and the luminescence was read in a BioTek FLx800 Fluorescence microplate reader to

determine the amount of firefly luciferase activity. To measure activity of the constitutively expressed *Renilla* luciferase as a control for transfection efficiency, Dual-Glo® Stop & Glo® Substrate was diluted 1:100 in Dual-Glo® Stop & Glo® Buffer. Of this, a volume equivalent to the original amount of DPBS present in the wells (75 µL) was added to the wells. Dual-Glo® Stop & Glo® Reagent contains coelenterazine, a substrate for *Renilla* luciferase that is converted to coelenteramide with the production of light (Figure 4B). Upon addition of the Dual-Glo® Stop & Glo® Reagent, the solution was allowed to incubate again at room temperature for 15 minutes, at which point the *Renilla* luminescence was measured. As a representation of the relative HIF-1 activity present in each cell type, a firefly/*Renilla* luminescence ratio was determined.

## **2.6 Gene expression analysis**

### *2.6.1 Sample preparation, RNA Extraction and Quality assessments*

Cells were grown in T25 flasks to 80 – 90% confluence, and harvested with trypsinization and placed in a 15 mL tube. The cell suspension was spun at 300 x g to form a cell pellet that was then washed with 5 mL DPBS and spun down a second time. The DPBS supernatant was aspirated off and the cell pellet was stored at -80°C until all samples were collected. RNA was extracted from cell pellets using the Arcturus PicoPure RNA Isolation Kit (Applied Biosystems, Carlsbad, CA, cat. #KIT0204) with 30 µL of elution buffer following DNase removal using the RNase-free DNase set (Qiagen, cat. # 79254). Aliquots were made at the time of isolation for the purposes of determining RNA integrity, concentration, and purity. The integrity and concentration of the RNA

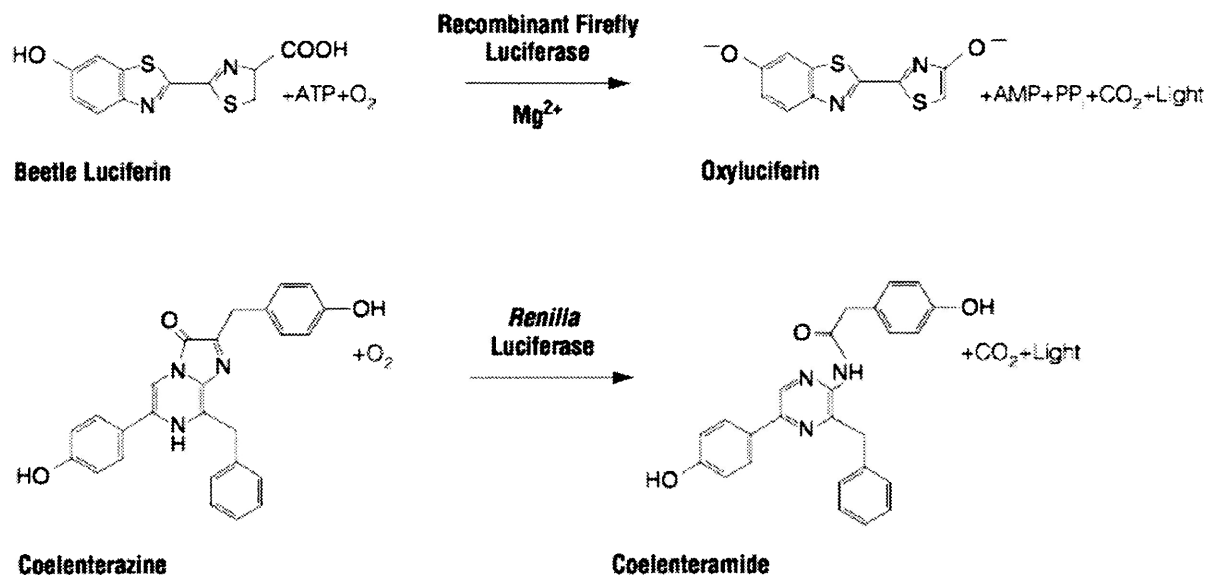


**Figure 4. Reactions catalyzed by firefly and *Renilla* luciferase.** (A) In the Dual-Glo® Luciferase Reagent, beetle luciferin is oxidized by firefly luciferase to produce oxyluciferin and light in the presence of Mg<sup>2+</sup>. (B) Coelenterazine in the Dual-Glo® Stop & Glo® Reagent is oxidized to coelenteramide by *Renilla* luciferase to produce light. Image acquired from datasheet for dual-glo® luciferase assay system (Promega cat. #E2920).

was measured using the BioRad Experion Automated Electrophoresis system with the StdSens Analysis Kit (BioRad, Hercules CA, cat. # 700-7111). RNA quality indicator (RQI) values were obtained based on the 28S:18S ratio, and only those samples with an  $RQI \geq 7.0$  were deemed acceptable for further analysis. The RNA purity was determined by an  $A_{260}/A_{280}$  absorbance ratio using a Synergy 4 plate reader (BioTek, Winooski, VT) with a Take-3 microvolume plate. Pure RNA samples, were accepted as having an  $A_{260/280} \geq 1.9$ , indicating low levels of protein contamination.

### *2.6.2 Conversion of RNA to cDNA*

Isolated RNA was converted to complementary DNA (cDNA) using the High Capacity cDNA Archive kit (Applied Biosystems, cat. #4368814). Final reaction volumes were 60  $\mu\text{L}$  containing 6  $\mu\text{L}$  RT buffer, 6  $\mu\text{L}$  primers, 2.4  $\mu\text{L}$  dNTPs, 3  $\mu\text{L}$  Multiscribe enzyme solution, 12.6  $\mu\text{L}$  nuclease-free water, and 30  $\mu\text{L}$  of sample RNA carried out in a nuclease-free 0.5  $\mu\text{L}$  PCR tube. A template-free control that contained only 30  $\mu\text{L}$  in lieu of sample RNA was also ran. Samples were placed in a 2720 Thermocycler (Applied Biosystems) and run for 10 minutes at 25°C, 120 minutes at 37°C, 5 minutes at 85°C, and cooled to 4°C.

### *2.6.3 Real-Time Polymerase Chain Reaction*

To quantify relative mRNA levels for a transcript of interest from reverse transcribed RNA, real-time polymerase chain reaction (RT-qPCR) was performed using a 7500 Real-Time PCR System (Applied Biosystems). Reaction mixtures were prepared again in 0.5  $\mu\text{L}$  nuclease-free PCR tubes containing 150 ng of cDNA, 45  $\mu\text{L}$  TaqMan

Gene Expression Master Mix (Applied Biosystems, cat. #4304437) and 4.5  $\mu$ L TaqMan Gene Expression assay (Applied Biosystems, Table 1). To bring the final volume of the mix up to 90  $\mu$ L, nuclease-free water was added. Technical triplicates were performed as 25  $\mu$ L fractions of the reaction mixture were added to 3 wells of a transparent MicroAmp Optical 96-Well Reaction Plate (Applied Biosystems, cat. # 4306737). The negative control reaction from cDNA preparation was also prepared for each plate that did not contain any cDNA but only nuclease-free water, as well as a positive tumour sample control to assess inter-plate variability. The cycle threshold ( $C_t$ ) was obtained for each transcript of interest and the Livak method (Livak and Schmittgen, 2001) was used to determine mRNA expression relative to the reference gene HPRT1 in each sample. HPRT1 was chosen as a reference gene based on previous studies that found it to remain unchanged in cells infected with HPV (DeCarlo, et al., 2008).

## 2.7 Statistical Analysis

All statistical analyses, as well as the production of figures were done using the open source programming language R (v3.1.0), in the RStudio integrated development environment (IDE). Data were tested for the parametric assumptions of normality and homogeneity of variance subjectively by histograms and box plots, respectively, and as well by the objective statistical tests, Shapiro-Wilks normality test and Bartlett test, respectively. Significance was set *a priori* as  $\alpha = 0.05$ . For statistical testing of experiments with two levels of one independent variable (IV), Student's t-test was used. Multi-way ANOVAs were used for experiments with more than two levels in IVs. Error bars above and below the arithmetic mean represent the standard deviation in all graphs.

**Table 1. TaqMan® (LifeTech) Gene Expression Assays**

<b>Gene ID</b>	<b>Assay ID</b>
HPRT1	HS99999909_m1
EPE6 Full-length	AI0IW1V
AAE6 Full-length	AIWR2XO
SLC2A1 (GLUT1)	HS00892681_m1
LDHA	HS00855332_g1
HK2	HS00606086_m1
PDK1	HS01561850_m1
VEGF-A	HS00900055_m1

## 3 RESULTS

### 3.1 Characterization of E6 variants used in this study

#### 3.1.1 Confirmation of variant specific SNPs

To study the effects of E6 variants on glucose metabolism, a two-donor approach was exploited in this study to consolidate the effects of E6 variants regardless of genetic background of the host. These two donors were used on separate occasions previously to study the differential ability of E6 variants to induce immortalization, transformation and migration of human keratinocytes (Richard et al., 2010, Niccoli et al., 2012). Prior to carrying out an investigation of E6 variant's effect on metabolism, E6 DNA that was previously retrovirally transduced into PHFKs (Donor One) was sequenced. Another member of the lab recently sequenced Donor Two and the correct SNPs for each variant were confirmed (Togtema, 2013). Sanger sequencing on PCR amplified E6 DNA was performed at Lakehead University's Paleo-DNA Laboratory and confirmed the appropriate SNPs present in cells harbouring each variant (Table 1, Appendix Figure A1 & A2).

#### 3.1.2 Relative E6 expression is equal between variants of each donor

To ensure that investigation into metabolic alterations by E6 variants was not due to varying levels of E6 gene expression, RT-qPCR was performed on E6 mRNA from cells harbouring the confirmed E6 variant. E6 expression from each donor and for each variant was similar (Figure 5). Thus, any effects of these variants on metabolism are not due to differences in E6 expression levels.

**Table 2. Detected SNPs in EPE6 and AAE6 from Donor One.**

<b>Cell Type</b>	<b>Predicted SNPs</b>	<b>Sequenced SNPs<sup>a</sup></b>
EPE6	0	0
AAE6	1) base 145, G -> T 2) base 286, T -> A 3) base 289, A -> G 4) base 335, C -> T 5) base 350, T -> G 6) base 532, A -> G	1) base 145, G -> T 2) base 286, T -> A 3) base 289, A -> G 4) base 335, C -> T 5) base 350, T -> G 6) Not detected <sup>b</sup>

<sup>a</sup>In reference to sequence ID NC\_001526.2

<sup>b</sup>This silent SNP is located in a region corresponding to the reverse E6 primer sequence and outside the range of the forward primer

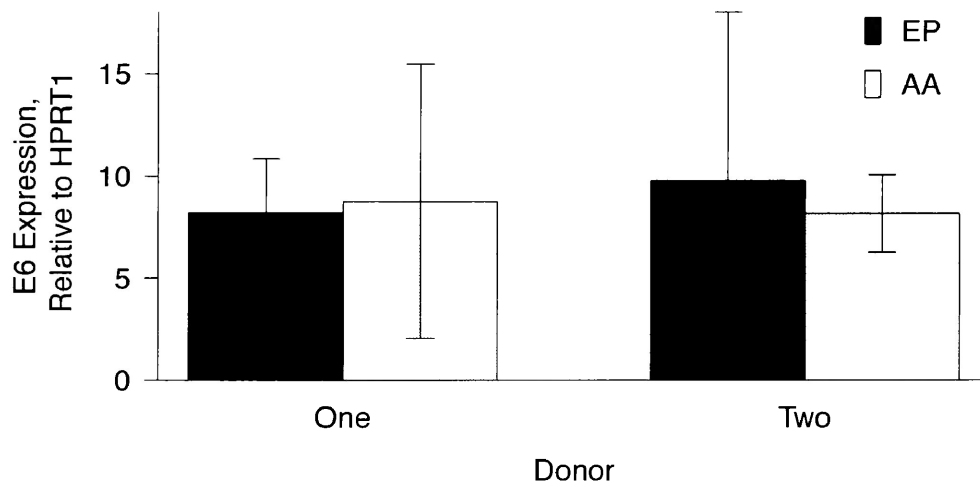


**Figure 5. E6 expression was similar between variants from each donor.** E6 expression was analyzed by RT-qPCR and E6 mRNA levels were similar between variants from each Donor. No significant difference in E6 expression was detected between donors ( $p = 0.830$ ) or variants ( $p = 0.816$ ). An interaction effect ( $p = 0.636$ ) was not found (Two-way ANOVA). The means +/- standard deviation are presented,  $n = 6$ .

### **3.2 Metabolic phenotype of cells transduced with E6 variants**

Previous work by our group has documented some of the differential effects on carcinogenesis by HPV16 E6 variants (Lichtig et al., 2006, Richard et al., 2010, Niccoli et al., 2012, Jackson et al., 2014). Of particular interest has been understanding the biology of the AA variant and how this may offer a malignant advantage over its EP counterpart. Protein analysis using 2D gel electrophoresis has found that, in the company of E7, the AAE6 variant led to alterations in the levels of several enzymes (upregulation of GAPDH, PKM2 and downregulation of IDH1 & 2, malate dehydrogenase) involved in glucose metabolism (Richard et al., 2010). These observations, alongside the epidemiological evidence of the HPV16 AA variant being a greater risk factor for invasion, lead to the hypothesis that AAE6 increased the Warburg effect since aerobic glycolysis promotes invasion (Gatenby et al., 2006, Lu et al., 2014). Thus, to determine whether AAE6 causes a metabolic shift reminiscent of a Warburg effect, glucose consumption and lactate production were measured in PHFKs transduced with each variant in two separate donors.

#### *3.2.1 Keratinocytes immortalized by AAE6 enhance glucose consumption in comparison to that of EPE6*

The consumption of glucose is often enhanced by cancer cells to ensure a continual supply of carbon needed for proliferation, while also increasing the amount of energy that can be obtained through a Warburg phenotype. To determine whether or not enhancement of glucose influx accompanied keratinocytes harbouring AAE6's production of lactate, a glucose analog having a fluorescent tag at the 2'-position was

used (2-NBDG). Cells were incubated with 2-NBDG, lysed, and the fluorescence was measured to determine if there was a difference in the ability of E6 variants to take up glucose. There was a significant increase in the normalized fluorescence of cell lysates of AAE6-transduced keratinocytes compared to EPE6 ( $p = 0.002$ , Figure 6). No significant difference between the donors ( $p = 0.206$ ) was found. The enhanced glucose consumption suggests the AAE6 variant induces a Warburg-type metabolism upon infection of host keratinocytes.

### *3.2.2 Lactate production is increased by keratinocytes immortalized by AAE6 in comparison to EPE6*

Using a tetrazolium-based assay on the growth media collected from each cell type, the amount of L-Lactate produced was determined. In this assay, LDHB is used to convert L-lactate that has been excreted into pyruvate, a reaction that produces NADH. The addition of diaphorase then uses the production of NADH to measure the conversion of tetrazolium to formazan, accompanied by a quantifiable colour change. The amount of lactate in the supernatant was significantly higher (~1.37-fold for Donor One, ~1.59-fold in Donor Two) in cells transduced with the AAE6 variant in comparison to EPE6 in both donors ( $p = 2.44 \times 10^{-6}$ , Figure 7). No significant difference between the donors ( $p = 0.657$ ) was found. These results suggest that upon infection with the AAE6 variant, metabolism is altered to produce more lactate, a hallmark of the Warburg effect that promotes invasion and metastasis (Gatenby et al., 2006). Collectively, the glucose consumption and lactate production increase in AAE6-transduced keratinocytes, regardless of donor, suggest AAE6 enhance the Warburg effect in host cells.

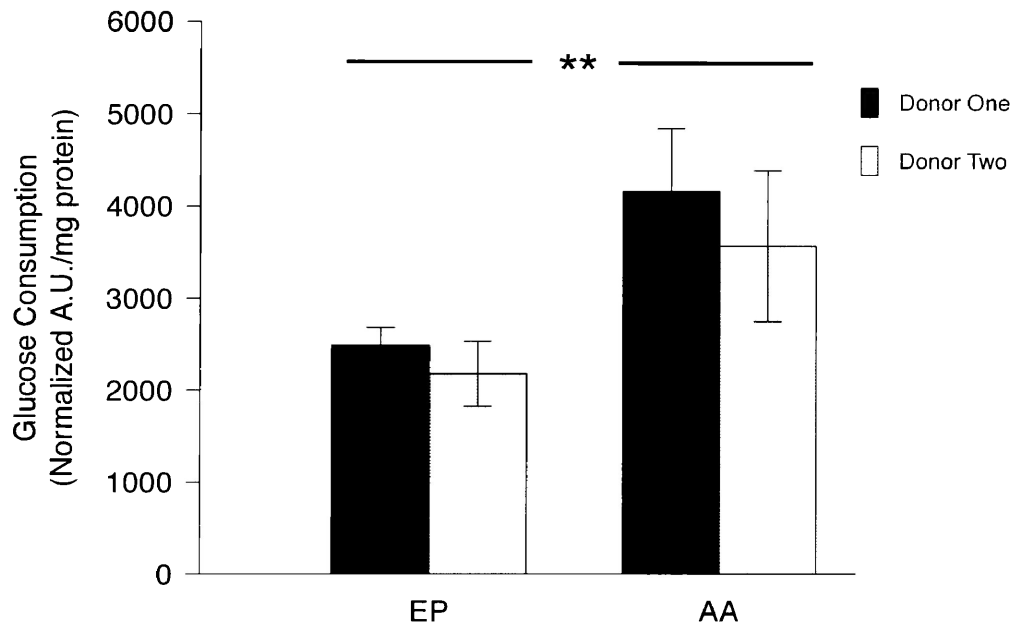


**Figure 6. Glucose Consumption of keratinocytes transduced with E6 variants.** AAE6-transduced keratinocytes take up significantly more 2-NBDG in comparison to EPE6-transduced keratinocytes ( $p = 0.002$ , Two-way ANOVA,  $n = 3$ ). No significant donor ( $p = 0.1142$ ) or interaction ( $p = 0.5920$ ) effects were found. The fluorescence of cell lysates from those treated with 2-NBDG was normalized to protein by Bradford assay and subtracted from that of a parallel well of cells not given 2-NBDG.

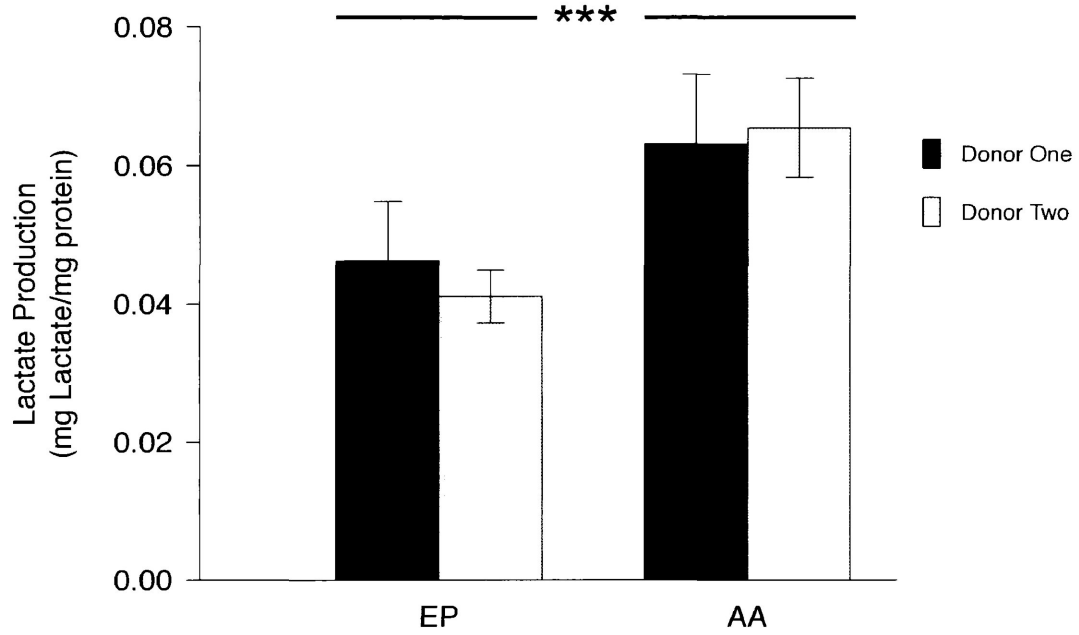


**Figure 7. Lactate production of keratinocytes transduced with E6 variants.** AAE6-transduced keratinocytes metabolize significantly more lactate in comparison to EPE6-transduced cells ( $p = 2.44 \times 10^{-6}$ , Two-way ANOVA,  $n = 6$ ). No significant donor ( $p = 0.657$ ) or interaction ( $p = 0.250$ ) effects were found. Lactate produced was normalized to the amount of protein by Bradford assay.

### **3.3 AAE6-transduced PHFKs increase HIF-1 $\alpha$ protein levels**

The metabolic phenotype of a Warburg effect can be brought about by several molecular mechanisms. These include, but are not limited to, alterations in pyruvate kinase isoform (PKM1 vs. PKM2) expression and activity, Akt stimulating the translocation of glucose transporters to the cell surface, dysfunction of TCA cycle enzymes, and the transcriptional enhancement of metabolic genes by c-myc or HIF-1 (Cairns et al., 2011). Previous results by our group have alluded to the possibility that HIF-1 transcriptional activity is enhanced by AAE6 based on evidence that protein levels of HIF-1 target genes (or their effectors) are altered in AAE6-transduced keratinocytes (Richard et al., 2010, Niccoli et al., 2012). Furthermore, overexpression of HIF-1 $\alpha$  is common in cancer (Zhong et al., 1999) and is associated with an increase in invasive potential and a poor prognosis (Semenza et al., 2003), including in cervical cancer (Birner et al., 2000, Huang et al., 2014). The increases in protein levels of HIF-1 targets, coupled with a metabolic phenotype reminiscent of the Warburg effect have provided strong evidence for HIF-1 activity to be enhanced by AAE6. Thus, the HIF-1 pathway was investigated in the context of these two E6 variants. Investigation into the HIF-1 pathway was carried out in Donor One only as both donors showed a similar metabolic phenotype, and these were the cells used previously to highlight AAE6's enhanced transformation potential (Niccoli et al., 2012).

#### *3.3.1 Whole cell lysates show HIF-1 $\alpha$ is enhanced in AAE6-transduced keratinocytes*

Induction of HIF-1 activity can be achieved by several mechanisms that act to induce HIF-1 $\alpha$  protein levels, while HIF-1 $\beta$  is constitutively expressed (Semenza, 2010).

Therefore, Western blot analysis was used to determine if HIF-1 $\alpha$  protein levels differed in the variant-transduced PHFKs. A positive control of HeLa cells treated with CoCl<sub>2</sub> was used as a HIF-1 $\alpha$  marker in Western blots to ensure technical parameters allowed for the detection of HIF-1 $\alpha$ . Under normoxic conditions, densitometry analysis revealed a significant increase in the relative protein levels of HIF-1 $\alpha$  normalized to the loading control,  $\beta$ -Actin, in AAE6-transduced keratinocytes in comparison to untransduced PHFKs (~3.9-fold,  $p = 0.022$ ) and EPE6-transduced keratinocytes (~2.7-fold,  $p = 0.042$ , Figure 7). No significant difference was found between EPE6-transduced keratinocytes and untransduced PHFKs ( $p = 0.848$ ). Thus, in the presence of the AAE6 variant, HIF-1 $\alpha$  accumulation in keratinocytes is seen compared to EPE6 and represents a potential novel function of this variant that may contribute to its increased risk for progression to invasive cervical cancer.

### *3.3.2 The nuclear pool of HIF-1 $\alpha$ is enriched by AAE6 in comparison to EPE6*

Following the translation of HIF-1 $\alpha$  mRNA to protein in the cytoplasm, it is readily degraded under normoxic conditions when a completely active HIF-1 $\alpha$ -degradation pathway is present. If HIF-1 $\alpha$  is not sufficiently degraded due to environmental hypoxia, inactivation of any one of the several regulators involved its degradation (i.e., prolyl hydroxylases or the von Hippel Lindau tumour suppressor protein), or an increase in the rate of HIF-1 $\alpha$  mRNA translation, it may translocate to the nucleus to dimerize with HIF-1 $\beta$  and become transcriptionally active.

The translocation of HIF-1 $\alpha$  is under the control of  $\alpha/\beta$  importins that regulate the

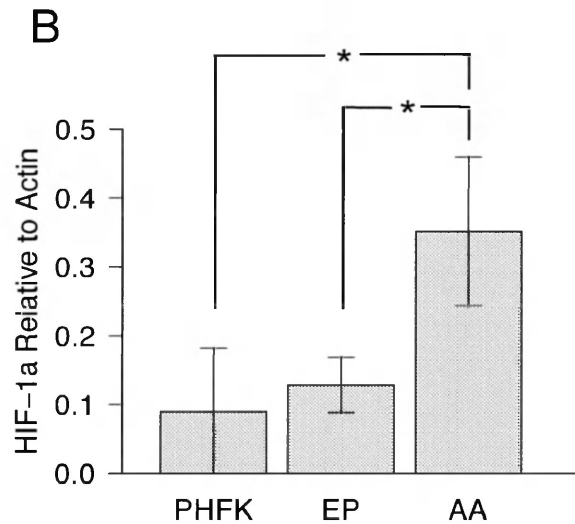
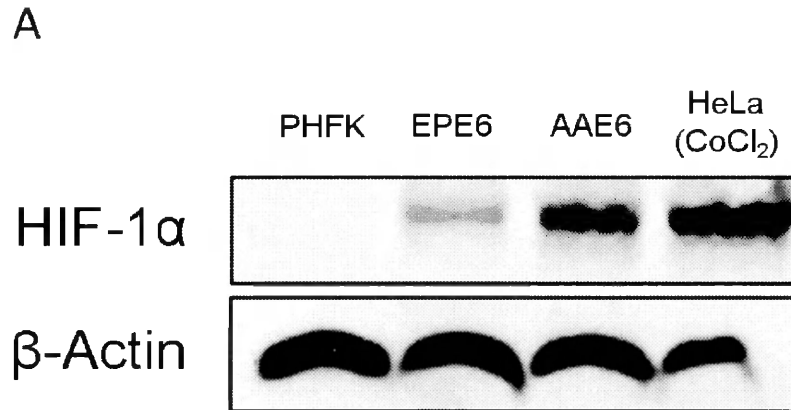


**Figure 8. Western blot analysis of HIF-1α protein levels in keratinocytes.** (A) Representative blot of three independent experiments showing HIF-1α increased in comparison to untransduced PHFKs and EPE6-transduced keratinocytes. Cobalt chloride treated (24 hour, 150 μM) HeLa cells served as a positive control of HIF-1α. (B) Densitometry analysis of relative levels of HIF-1α normalized to the housekeeping protein β-Actin. AAE6 cells show significantly more HIF-1α in comparison to EPE6 cells ( $p = 0.042$ ) and untransduced PHFKs ( $p = 0.022$ , Tukey-HSD test,  $n = 3$ ).

transport of several proteins with an NLS sequence across the nuclear membrane (Depping et al., 2008). Thus, to investigate whether or not the differences in HIF-1 $\alpha$  protein levels were also found in the nucleus, Western blotting on subcellular fractions was performed. The majority of HIF-1 $\alpha$  detected was located in the nucleus and little (in some trials, none) was detectable in the cytoplasm (Figure 8A). Densitometry revealed a significant increase ( $p = 0.031$ ) in the amount of HIF-1 $\alpha$  detected in AAE6 cells in the nucleus but not in the cytoplasm ( $p = 0.837$ ), relative to their respective subcellular loading controls (Figure 8B). Therefore, the HIF-1 $\alpha$  detected in both AAE6 and EPE6-transduced keratinocytes resides primarily in the nucleus, where it may dimerize with its transcriptional co-activators and proceed to transactivate its target genes.

### **3.4 Luciferase reporter assay for HIF-1 reveals HIF-1 transcriptional activity is enhanced under hypoxia in AAE6-transduced keratinocytes.**

Upon translocation to the nucleus, HIF-1 $\alpha$  can dimerize with HIF-1 $\beta$ , followed by transcription complex formation with p300/CBP (Semenza, 2003). Subsequent binding of the HIF-1 $\alpha$ /HIF-1 $\beta$ /p300 transcription factor complex to HREs in the promoter sequence of target genes results in augmentation of their transcription. To determine whether the enhanced HIF-1 $\alpha$  protein level present in AAE6-transduced keratinocytes causes an increase in the transcriptional activity of HIF-1, a luciferase reporter assay was used. A plasmid encoding the firefly luciferase gene sequence under the control of a HIF-1-inducible promoter was cotransfected with a constitutively active *Renilla* luciferase gene for transfection normalization. Enzymatic activity of each luciferase is then quantified to determine the ability of HIF-1 to induce transcription of HIF-1-responsive genes.

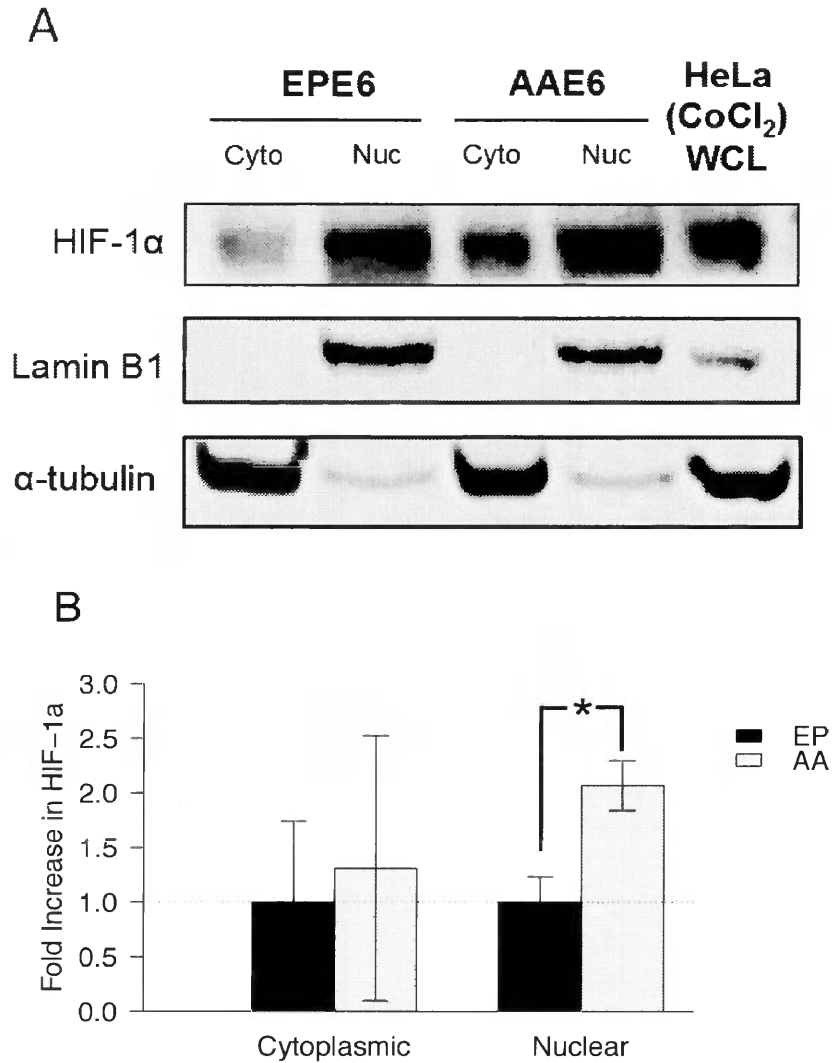


**Figure 9. Western blot analysis of subcellular fractions of HIF-1α protein.** (A) Representative blot of three independent experiments showing HIF-1α nuclear pool increased in AAE6-transduced keratinocytes. A whole cell lysate of cobalt chloride treated (24 hour, 150 μM) HeLa cells served as a positive control of HIF-1α. (B) Densitometry analysis of relative levels of HIF-1α normalized to subcellular housekeeping proteins. AAE6 cells show significantly more HIF-1α in comparison to EPE6 cells in nuclear ( $p = 0.031$ ) but not in cytoplasmic ( $p = 0.837$ ) fractions (Student's t-test,  $n = 3$ ).

### 3.4.1 GFP transfection optimization

Prior to HIF-1 activity determination, confirmation of transfection had to be carried out. To do this, a constitutively active GFP plasmid included with the Cignal™ firefly and *Renilla* plasmids was used. Several transfection reagents and variable amounts of plasmid were used to qualitatively determine the optimal amounts of each for a successful transfection. Several commercially available transfection reagents were tried (Fugene 6, HiPerfect, Attractene, Mirus2020 and Mirus X2) with variable amounts of transfection reagent and DNA. Finally, both Mirus 2020 and Mirus X2 transfection reagents similarly gave the best transfection efficiency (~10% for both EPE6 and AAE6) with the lowest cytotoxicity using a volume of 0.20 µL/100 µL cell suspension and 100 ng of plasmid (Figure 10). No increase in transfection efficiency was observed when plasmid amount increased (data not shown).

### 3.4.2 HIF-1 activity is enhanced under hypoxia in AAE6-transduced keratinocytes in comparison to EPE6-transduced keratinocytes

Following the transfection optimization, luciferase assays were performed under both ambient oxygen and hypoxia. This was done to determine if HIF-1 activity was altered between variants under the normoxic conditions where a difference in HIF-1 $\alpha$  protein was detected, as well as the hypoxic environment found in many tumours (Wilson & Hay, 2011). No difference in firefly/*Renilla* luciferase activity ratio between cell types was observed under normoxia ( $p = 0.604$ , Figure 11). However, a significant increase was observed in the ratio for AAE6-transduced keratinocytes in comparison to EPE6 under hypoxia ( $p = 0.017$ ).

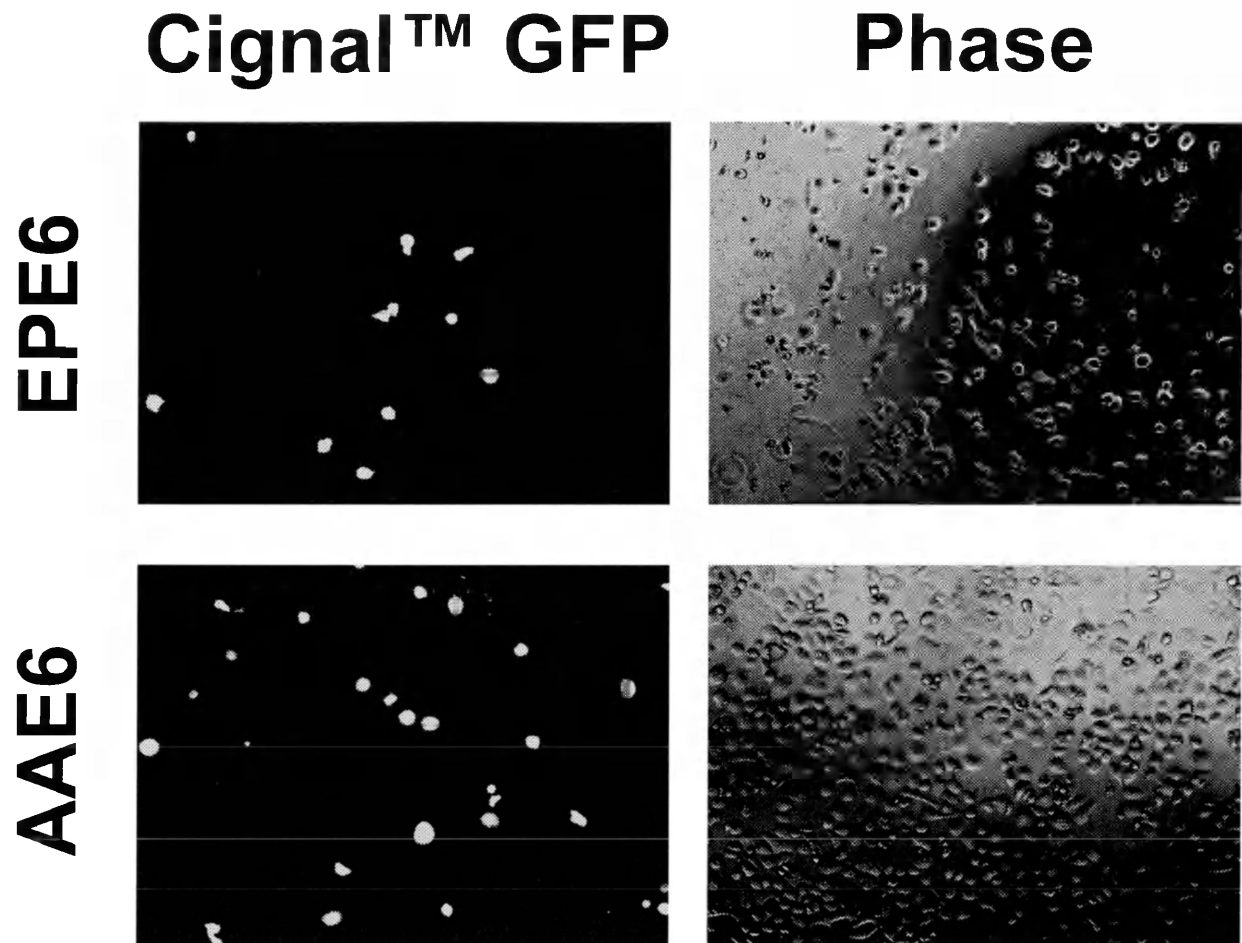


**Figure 10. Confirmation of Signal™ reporter plasmid transfection.** Representative image of Signal™ GFP positive control plasmid, that was used to determine the optimal transfection reagent, volume, and amount of DNA to use to transfect luciferase reporter plasmids. Shown here, Mirus reagents gave the best transfection efficiency (~10% in both cell types) with the lowest cytotoxicity.

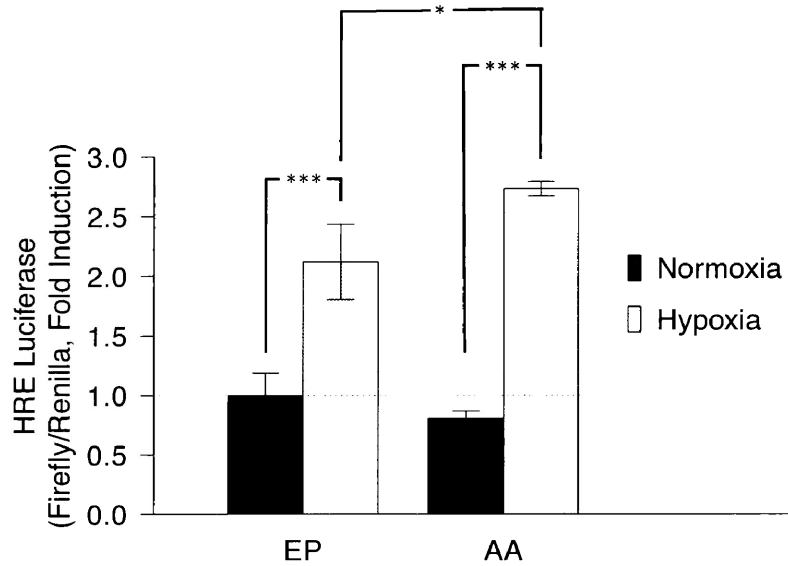


**Figure 11. AAE6 induces HRE-responsive Luciferase activity to a greater degree under hypoxia.** HRE Luciferase activity (normalized to *Renilla*) was significantly increased under hypoxia for both EPE6 ( $p = 4.05 \times 10^{-4}$ ) and AAE6 ( $p = 7.5 \times 10^{-6}$ ). Luciferase activity was significantly greater in AAE6 under hypoxia in comparison to EPE6 ( $p = 0.017$ , Tukey HSD). The means +/- standard deviation are shown,  $n = 3$ .

### 3.5 Transactivation of HIF-1 target genes in variant transduced keratinocytes

It has been estimated that HIF-1 activates the transcription of nearly 100 genes involved in metabolism, angiogenesis, cell survival, and invasion (Semenza, 2003). With evidence that HIF-1 protein levels and activity under hypoxia are enhanced in AAE6, whether the transactivation of HIF-1 target genes was responsible for the observation of an enhanced Warburg effect by AAE6 was investigated. Using RT-qPCR, the relative expression of HIF-1 target genes involved in this metabolic shift including glucose transporter 1 (GLUT1), Hexokinase II (HK2), lactate dehydrogenase A (LDHA) and pyruvate dehydrogenase kinase 1 (PDK1) were assayed. The expression of VEGF-A was also examined as a classical HIF-1 target gene responsible for tumour angiogenesis. Again, gene expression was studied both under normoxia and hypoxia as promoter activity analysis revealed a significant increase in HIF-1 activity only under hypoxic conditions.

As stated previously, an increase in the rate of glucose consumption is a hallmark of most proliferating cells. The facilitative glucose transporter proteins, GLUT1 – 9, control the increased uptake of glucose in cancer cells (Levine & Puzio-Kuter, 2010). HIF-1 activates the transcription of GLUT1 and GLUT3 in several cancers to facilitate the increased requirement for glucose for proliferation and cell survival (Semenza, 2010). Given that AAE6 induced an increase in glucose consumption, GLUT1 expression was measured both under ambient air conditions (normoxia) and hypoxia (Figure 12A). Two-way ANOVA revealed a significant increase in GLUT1 expression for AAE6 ( $p = 0.022$ ) and under hypoxia ( $p = 5.26 \times 10^{-6}$ ) as well as an interaction effect ( $p = 0.006$ ) indicating a differential response of the variants between the two oxygen levels tested. Post-hoc

analysis revealed a significant increase in GLUT1 expression under hypoxia in AAE6 keratinocytes compared to EPE6 ( $p = 0.008$ ). The hypoxic induction of GLUT1 expression was ~1.9-fold higher in AAE6 compared to EPE6 (Figure 12B).

Upon transport into the cell by facilitated glucose transport, glucose is phosphorylated at the 6'-position by hexokinase I, II, or III. Hexokinase I and II are target genes of HIF-1 and HK2 upregulation is closely associated with a Warburg metabolism (Mathupala et al., 2009), so it represented an interesting HIF-1 target gene to investigate in the context of the E6 variants. Again, the expression of HK2 was analyzed both under normoxia and hypoxia (Figure 13A). In this case, only a significant difference was found between hypoxia and normoxia ( $p = 3.68 \times 10^{-6}$ ) with no difference between the variants ( $p = 0.200$ ) or interaction effect ( $p = 0.636$ ). The hypoxic induction of HK2 expression did not yield a significant difference between the variants ( $p = 0.728$ , Figure 13B).

The production of lactate is one of the key features of the Warburg effect. The synthesis of lactate from pyruvate is catalyzed by LDHA and thus represents an additional interesting HIF-1 target with regards to the Warburg effect. Surprisingly, LDHA expression was lower in AAE6 than in EPE6 ( $p = 0.030$ ), along with the expected significant main effect of oxygen levels ( $p = 7.51 \times 10^{-6}$ ). However, no interaction effect ( $p = 0.480$ ) was found, indicating that the intrinsic levels of LDHA gene expression are higher in EP (Figure 14A). However, the extent of hypoxic induction of LDHA mRNA was higher in AAE6 (Figure 14B), albeit not significantly ( $p = 0.169$ ).

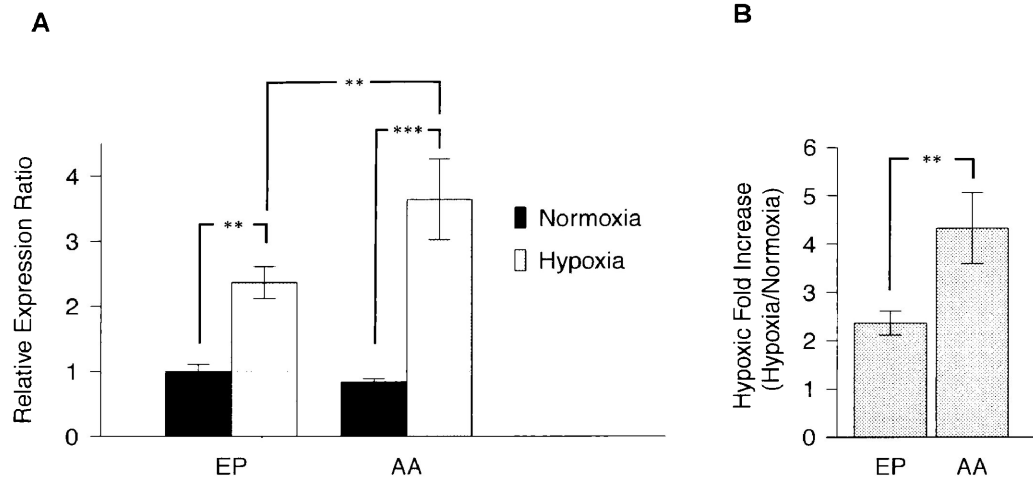


**Figure 12. Relative GLUT1 mRNA levels in E6-transduced keratinocytes under normoxic and hypoxic conditions.** (A) GLUT1 expression was significantly higher under hypoxia in comparison to normoxia for both EPE6 ( $p = 0.005$ ) and AAE6 ( $p = 3.60 \times 10^{-4}$ ). AAE6 showed significantly higher expression of GLUT1 in comparison to EP under hypoxia ( $p = 0.008$ , Two-Way ANOVA with Tukey HSD post-hoc). (B) The hypoxic response of GLUT1 expression in comparison to normoxia was greater in AAE6 cells than EPE6 cells ( $p = 0.011$ , Student's t-test). The means  $\pm$  standard deviation are presented,  $n = 3$ .

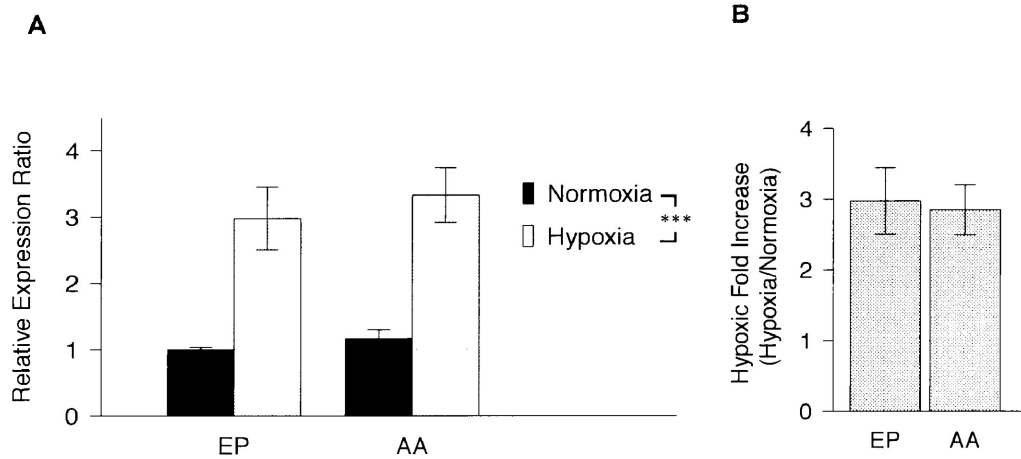


**Figure 13. Relative HK2 mRNA levels in E6-transduced keratinocytes under normoxic and hypoxic conditions.** (A) HK2 expression was significantly higher under hypoxia ( $p = 3.68 \times 10^{-6}$ ) with no variant differences ( $p = 0.200$ ) or interaction ( $p = 0.636$ , Two-Way ANOVA) effect. (B) The hypoxic response of HK2 expression in comparison to normoxia was similar between variants ( $p = 0.728$ ). The means  $\pm$  standard deviation are presented,  $n = 3$ .

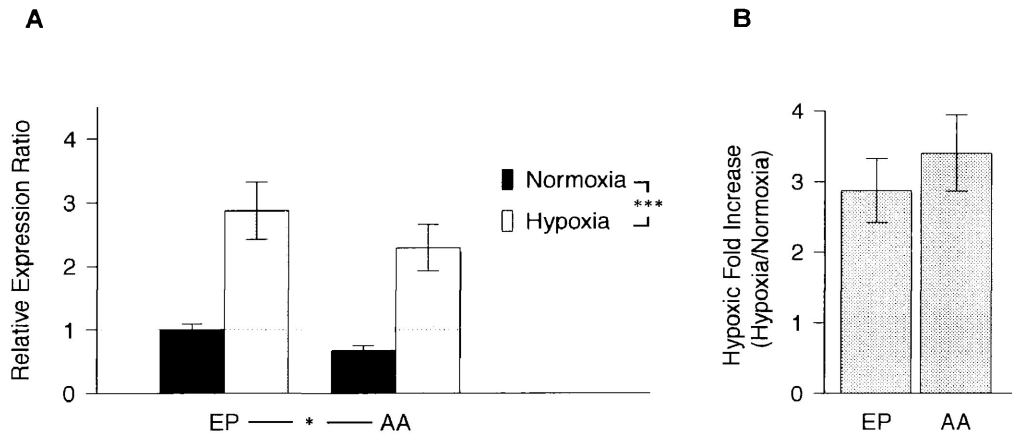


**Figure 14. Relative LDHA mRNA levels in E6-transduced keratinocytes under normoxic and hypoxic conditions.** (A) LDHA expression was significantly higher under hypoxia ( $p = 7.51 \times 10^{-6}$ ) and in EPE6 ( $p = 0.030$ ) but no interaction effect ( $p = 0.480$ , Two-Way ANOVA) was found. (B) The hypoxic induction of LDHA expression was higher in AAE6 but not significantly ( $p = 0.264$ ). The means  $\pm$  standard deviation are presented,  $n = 3$ .

In addition to LDHA, PDK1 also regulates the metabolic fate of pyruvate and increases lactate production. PDK1 phosphorylates pyruvate dehydrogenase (PDH), inhibiting its ability to metabolize pyruvate into acetyl Co-A. An increase in PDK1 expression is recognized as a HIF-1-regulated metabolic shift required for adaptation to hypoxia (Kim et al., 2006). PDK1 expression was slightly increased in AAE6, although this was not statistically significant ( $p = 0.177$ , Figure 15A). Again, hypoxia significantly increased ( $p = 3.58 \times 10^{-6}$ ) PDK1 expression with no interaction effect ( $p = 0.323$ ). The hypoxic induction of was higher in AAE6, although not significantly ( $p = 0.264$ , Figure 15B).

Along with genes involved in metabolism, HIF-1 also transactivates the expression of proangiogenic genes. Vascular endothelial growth factor-A (VEGF)-A is an HIF-1 target that interacts with its cognate receptor, VEGFR that is expressed solely on endothelial cells and stimulates their proliferation, forming new blood vessels (Lee et al., 2004). Induction of angiogenesis via HIF-1 is an integral part of a tumour's ability to adapt to the intratumoural hypoxia that accompanies cell proliferation. If tumours do not have access to a blood supply, sufficient nutrients cannot be obtained for sustained proliferation and survival, so it is not surprising that inhibition of angiogenesis is associated with a decrease in the rate of tumour growth and progression (reviewed in Liao & Johnson, 2007). Therefore, VEGF-A expression was examined in the context of E6 variants under hypoxia and normoxia. Two-way ANOVA again revealed VEGF-A expression was significantly higher under hypoxia ( $p = 6.98 \times 10^{-8}$ ) but no difference between variants was found ( $p = 0.098$ , Figure 16A). While a significant interaction effect was found ( $p = 0.043$ ), post-hoc analysis (Tukey HSD test) did not find any

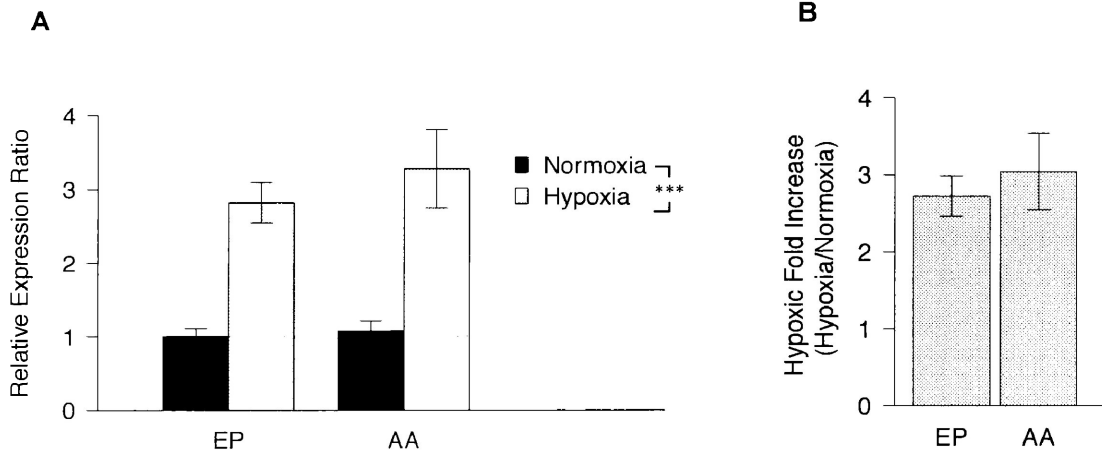


**Figure 15. Relative PDK1 mRNA levels in E6-transduced keratinocytes under normoxic and hypoxic conditions.** (A) PDK1 expression was only significantly higher under hypoxia ( $p = 3.58 \times 10^{-6}$ ) with no significant variant ( $p = 0.177$ ) or interaction effect ( $p = 0.323$ , Two-Way ANOVA) (B) The hypoxic induction of PDK1 expression was not significantly greater in AAE6 cells than EPE6 cells ( $p = 0.3959$ , Student's t-test). The means +/- standard deviation are presented,  $n = 3$ .

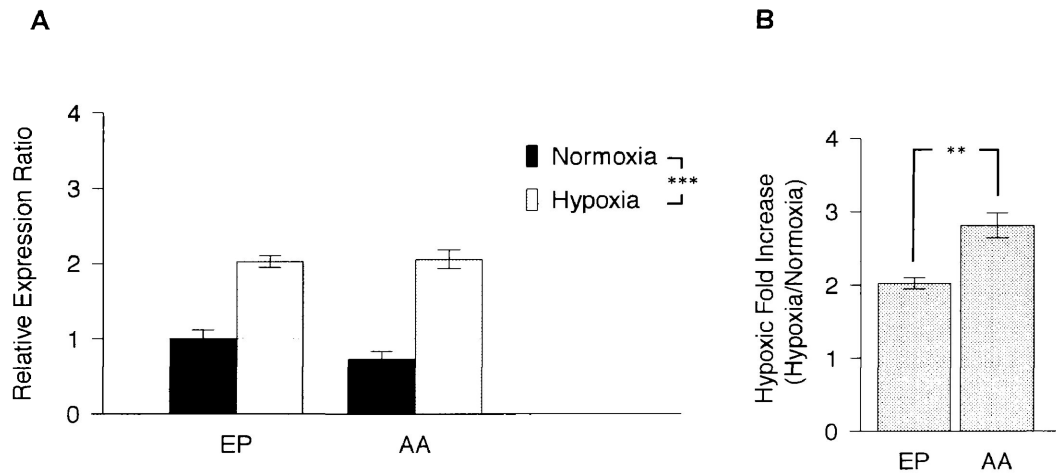


**Figure 16. Relative VEGF-A mRNA levels in E6-transduced keratinocytes under normoxic and hypoxic conditions.** (A) VEGF-A expression in Donor One was greater under hypoxia ( $p = 6.98 \times 10^{-8}$ ) with difference between variants ( $p = 0.098$ ), although an interaction effect was found ( $p = 0.043$ , Two-Way ANOVA). However, Tukey HSD post-hoc analysis revealed no significant differences between cell types at the same oxygen level. (B) The hypoxic induction of VEGF-A expression was significantly greater in AAE6 in comparison to EPE6 ( $p = 0.002$ ). The means  $\pm$  standard deviation are shown,  $n = 3$ .

significant differences between variants at the same oxygen level. However, the induction of VEGF-A expression under hypoxia (Figure 16B) was significantly higher in AAE6 ( $p = 0.006$ ).

## 4 DISCUSSION

### 4.1 The AAE6 variant of HPV16 enhances the Warburg effect in transduced keratinocytes

In this study, the glucose metabolism of cells that express two common variants with different risk factors for invasive cervical cancer was investigated. An increase in glucose consumption and subsequent production of lactate are hallmarks of cancer cells (Hanahan & Weinberg, 2011). Furthermore, the alteration of glucose metabolism is a unifying theme of oncogenic viruses (Noch & Khalili, 2012). In this study, a metabolic shift was found in AAE6-transduced keratinocytes in accordance with a Warburg effect as both glucose consumption and lactate production were enhanced by AAE6 over EPE6. Therefore, the alternative hypothesis put forth at the onset of this study that there is a difference in the Warburg effect between host cells with each variant is valid. These findings have several implications that may help to explain the differential ability of these two common HPV16 variants in tumour progression.

It has been recently postulated that a Warburg metabolism supports increased proliferation as it provides increased carbon for anabolic processes without the production of growth inhibitory ROS typical of oxidative phosphorylation (Vander Heiden, 2009). The results reported herein support this hypothesis as AAE6 displays the metabolic phenotype of a Warburg effect, as well as decreases the doubling time when

transduced into PHFKs compared to EPE6 (Richard et al., 2010, Niccoli et al., 2012). In addition to enhancing proliferation, the Warburg effect may contribute to AAE6's ability to promote malignant transformation (the process by which normal cells acquire the properties of cancer) of immortalized keratinocytes (Niccoli et al., 2012). While it is well understood that the Warburg effect by itself is not sufficient to cause transformation, it does appear to be a requirement for transformation to occur (Kim & Dang, 2006). Furthermore, aerobic glycolysis also contributes to extracellular acidification, a condition promoting clonal selection (selection for cancer cells over their non-transformed counterparts), local invasion, and tumour progression (Gatenby et al., 2006, Estrella et al, 2013). With evidence here for enhanced lactate production in AAE6 transduced cells, it is possible that this altered metabolism may contribute to AA variants' increased risk for progression to high grade intraepithelial neoplasia (Xi et al., 2007) and invasive cervical cancer (Berumen et al., 2001).

#### **4.2 Enhanced levels of HIF-1 $\alpha$ protein in AAE6-transduced keratinocytes**

Enhanced glucose uptake and lactate production are two common characteristics of aggressive cancers that may arise by several mechanisms that act to induce the transcription of genes involved in metabolism, or by altering enzyme activity (Cairns et al., 2011). HIF-1 protein levels and activity are commonly enhanced in cancers through various mechanisms to transcriptionally increase a wide array of genes involved in cancer progression, including those responsible for the Warburg effect (Semenza et al., 2010). Thus, HIF-1 represented a plausible explanation for the enhanced Warburg effect observed in AAE6-transduced keratinocytes based on previous findings that the protein

levels of HIF-1 targets (GAPDH, PKM2, CA9) or proteins influenced by HIF-1 target genes (E-cadherin) differ between AAE6- and EPE6-transduced keratinocytes (Richard et al., 2010, Niccoli et al., 2012). In accordance with this hypothesis, HIF-1 $\alpha$  protein levels were enhanced in AAE6-transduced keratinocytes. Furthermore, control of the nuclear localization of several transcription factors is an important step in the regulation of their activity (Darnell, 2002). While HIF-1 $\beta$  is constitutively expressed in the nucleus, HIF-1 $\alpha$  translocation to the nucleus is an important step in its regulation and is achieved by inhibiting its proteasomal dependent breakdown (Chilov et al., 1999), or increasing its synthesis by the PI3K/Akt (Laughner et al., 2001) or p42/p44 MAPK pathways (Mills et al., 2009). By separating the nuclear and cytoplasmic portions of cells, it was determined the majority of the HIF-1 $\alpha$  protein detected in whole cell lysates resides in the nucleus, indicating that regulation of HIF-1 $\alpha$  nuclear translocation did not represent a significant barrier to any changes in its activity in keratinocytes harbouring either variant.

The underlying cause of increased HIF-1 $\alpha$  may stem from any of the mechanisms acting on its translation or inhibiting its protein breakdown. Both the classical MAPK and PI3K/Akt pathways act to induce the translation of HIF-1 $\alpha$  mRNA into protein by inducing the eukaryotic translation initiation factor (eIF-4E) and p70S6-kinase that are involved in the synthesis of many proteins, including HIF-1 $\alpha$  (Semenza 2003, Sonenberg & Gingras, 1998). The underlying cause of HIF-1 $\alpha$  protein accumulation in AAE6-transduced cells may result from activation of the MAPK pathway as a L83V substitution in the amino acid sequence of E6 (one of those found in AAE6) activates this pathway (Chakrabarti et al., 2004). Conversely, some viral oncoproteins inhibit HIF-1 $\alpha$  breakdown by direct protein-protein interactions with HIF-1 $\alpha$  itself, the PHDs, or VHL

(Cunningham et al., 2014). AAE6 may bind to any of these proteins may inhibit HIF-1 $\alpha$  breakdown and therefore, increase its protein levels.

### **4.3 Hypoxia as a requirement to enhance HIF-1 activity in AAE6 transduced keratinocytes**

To assess whether or not the increase in HIF-1 $\alpha$  protein levels was sufficient to induce an increase in transcription of HIF-1 target genes and a Warburg effect, a luciferase assay was first used to specifically assess HIF-1 promoter activity. Surprisingly, a difference in HIF-1 promoter activity between variants was only observed under hypoxia, while no difference was observed between variants for cells assessed under normoxia even though a difference in protein levels was found. The requirement for hypoxia to induce a difference in promoter activity could be mitigated by factor inhibiting hypoxia-inducible factor 1 (FIH-1). FIH-1 is an O<sub>2</sub>-dependent asparaginyl hydroxylase that hydroxylates HIF-1 at Asn-803 under normoxia, preventing it from binding to its requisite transcriptional coactivator, p300 (Lando et al., 2002). Therefore, while HIF-1 $\alpha$  protein levels are higher in AAE6-transduced keratinocytes, perhaps a functional difference in its promoter activity is not observed due to asparaginyl hydroxylation that is relieved only by hypoxia. Future investigations can test this hypothesis by using RNA interference directed toward FIH-1 under normoxia and observe if the same enhancement of HIF-1 activity is found. Furthermore, the difference in activity under hypoxia may be due not to differences in HIF-1 protein levels, but once dehydroxylated by repression of FIH-1, the E6 variants may differentially bind to p300. HPV16 E6 binds to p300 and inhibits its ability to activate p300-responsive promoters,

while several mutants of EPE6 do not bind p300 (Patel et al., 1999). A differential ability of AAE6 versus that of EPE6 may represent a contributing factor to the difference in HIF-1 responsive promoter activity under hypoxia.

With the knowledge that HIF-1 promoter activity was enhanced under hypoxia, the expression of some HIF-1 responsive genes involved in metabolism and angiogenesis was then analyzed by RT-qPCR. In agreement with HRE-coupled luciferase assays to assess HIF-1 activity, mRNA levels of GLUT1, HK2, LDHA, PDK1 and VEGF-A were similar between variants under normoxia. Therefore, the second alternative hypothesis, that enhanced aerobic glycolysis is due to increased HIF-1 activity, is not supported based on gene expression analysis. However, it was found that GLUT1 expression was significantly higher in AAE6 in comparison to EPE6-transduced keratinocytes under hypoxia. The hypoxic response in AAE6 cells was significantly higher for both GLUT1 and VEGF-A, and slightly increased (albeit not statistically significant) in the case of LDHA and PDK1, in comparison to normoxic controls of each variant cell type. Counter-intuitive to the lactate production results, LDHA expression was decreased in AAE6 cells. Since the magnitude of lactate production was higher in Donor Two between AAE6 and EPE6, future studies can investigate if this difference in LDHA expression is also found in Donor Two. These results, coupled with HIF-1 promoter assay investigations, suggest that the enhanced ability to induce HIF-1 target genes may represent a possible adaptive advantage to the hypoxic tumour microenvironment by the AA variant in comparison to EP. This adaptive advantage may partially explain AA's increased risk for the development of high-grade intraepithelial lesions (Xi et al., 2007) and cervical cancer (Berumen et al., 2001). HIF-1 expression and activity is associated with enhanced cancer

progression owing to its ability to increase the expression of several genes (in addition to those investigated in this study) involved in cellular proliferation and survival, metabolism, epithelial-mesenchymal transition, invasion, and metastasis (reviewed in Semenza, 2012). The specific genes and the level of their induction during hypoxia are not ubiquitous and human cancers display some variation in the battery of HIF-1 target genes induced by hypoxia (Chi et al., 2006). It is likely that HIF-1 target genes are differentially regulated between variant cell types, which may explain why GLUT1 is expressed to a greater degree under hypoxia in AAE6 cells, but other genes investigated were not.

While the enhanced transcriptional activity of HIF-1 under hypoxia is an interesting finding, the similarity in HIF-1 promoter activity and the expression of genes involved in metabolism under normoxia suggests that additional mechanisms are likely attributable to the enhanced Warburg effect in AAE6-transduced keratinocytes. While some mechanisms that induce a Warburg effect can be ruled out as they also act by transcription on HIF-1 target genes (e.g., c-myc activation), additional mechanisms may be affected by AAE6 that act post-transcriptionally on glycolytic enzymes. For example, studies have found activated Akt via the PI3K pathway can induce glucose uptake by enhancing GLUT1 protein trafficking to the cell membrane, but not affecting its protein level (Rathmell et al., 2003). Active Akt also increases the activity of other glycolytic enzymes, such as hexokinase II via post-translational mechanisms (Cairnes et al., 2011). Since Akt activation also induces HIF-1 $\alpha$  synthesis, this could be an underlying upstream mechanism explaining both the Warburg effect and enhanced HIF-1 $\alpha$  protein levels in AAE6.

As an alternative to Akt-mediated activation of aerobic glycolysis, other mechanisms may also be contributing to an enhanced Warburg effect. Regulation of PKM2 activity between its highly active tetrameric form and less-active dimeric form can be achieved in multiple ways that affect lactate production (Hitosugi et al., 2009). OCT-1 is a transcription factor that can control pyruvate fate by enhancing transcription of metabolic genes not investigated in this study (e.g., PDK4) (Shakya et al., 2009). Conversely, AMP-activated protein kinase (AMPK) may increase lactate production by directly activating PDK1 activity, without affecting its protein level (Wu et al., 2013). Other post-translational modifications on several glycolytic enzymes, such as phosphorylation of hexokinase 2, phosphofructokinase-2, pyruvate dehydrogenase and LDHA all promote aerobic glycolysis by altering the activity of these enzymes (reviewed in Upadhyay et al., 2013). Furthermore, it has recently been found that lactate production can be achieved via increased glutamine consumption and conversion to pyruvate through the TCA cycle, representing a potential pathway not reliant on glycolysis for lactate production (Koppenol et al., 2011). Collectively, activation of one (or a combination) of these pathways may provide alternative explanations for the observed aerobic glycolysis found in this study. Nonetheless, the enhanced aerobic glycolysis and increased HIF-1 activity under hypoxia by AAE6 found herein represent two novel findings that represent potential contributing factors to AA's enhanced tumourigenic capability.

## 5 CONCLUSIONS AND FUTURE DIRECTIONS

In this study, the glycolytic phenotype of PHFKs transduced with either the AA or EP HPV16 E6 oncogene was established. Cells with AAE6 appear to take up more glucose and produce more lactate than do EPE6-transduced keratinocytes. Furthermore, a potential regulator of this metabolic shift, HIF-1, was also investigated to determine if the Warburg effect was the result of enhanced HIF-1 activity. Interestingly, although more HIF-1 $\alpha$  protein was detected by Western blotting in AAE6-transduced keratinocytes under normoxia, this difference did not result in more HIF-1 activity at the same oxygen tension. However, HIF-1 activity was significantly increased under hypoxia and the response of GLUT1 and VEGF-A expression to hypoxia was greater in AAE6-transduced keratinocytes. These results suggest that AAE6 may induce an adaptive advantage to hypoxia, which is typical of a tumour microenvironment. This adaptive advantage may then provide a contribution to the AA variant's documented increased risk for the development of cervical cancer.

These results open the door for further investigations regarding the functional increase in aerobic glycolysis and HIF-1 activity under hypoxia by AAE6. Firstly, inhibition studies on glucose transport using non-hydrolyzable substrates of glucose can answer whether or not this metabolic phenotype is a requirement for AAE6's enhanced *in vitro* capacity for immortalization, transformation, and invasion, as reported previously by our group. If this is not the case, a similar approach examining glutamine metabolism in variant-transduced cells can be explored, due to an increasing number of reports highlighting the significance of glutamine metabolism on lactate production and proliferation. Additionally, the enhanced HIF-1 activity under hypoxia should be

investigated as to whether or not it has any functional significance regarding AAE6's ability to induce migration and invasion under the hypoxic conditions typical of a tumour microenvironment. These follow-up studies will answer whether or not the results described in this study have a bearing on AAE6's enhanced tumourigenicity.

## 6 REFERENCES

- Agani, F., Jiang, B.H., 2013. Oxygen-independent Regulation of HIF-1: Novel Involvement of PI3K/AKT/mTOR Pathway in Cancer. *Curr. Cancer Drug Targets*. 13, 245–251.
- Bersten, D.C., Sullivan, A.E., Peet, D.J., Whitelaw, M.L., 2013. bHLH-PAS proteins in cancer. *Nat. Rev. Cancer*. 13, 827–841.
- Berumen, J., Ordoñez, R. M., Lazcano, E., Salmeron, J., Galvan, S. C., Estrada, R. A., Yunes, E., Garcia-Carranca, A., Gonzalez-Lira, G., Madrigal-de la Campa, A. 2001. Asian-American variants of human papillomavirus 16 and risk for cervical cancer: a case–control study. *Journal Natl Cancer I*. 93, 1325-1330.
- Birner, P., Schindl, M., Obermair, A., Plank, C., Breitenecker, G., Oberhuber, G. 2000. Overexpression of hypoxia-inducible factor 1 $\alpha$  is a marker for an unfavorable prognosis in early-stage invasive cervical cancer. *Cancer Res*. 60, 4693-4696.
- Bruick, R.K., McKnight, S.L., 2001. A conserved family of prolyl-4-hydroxylases that modify HIF. *Science*. 294, 1337–1340.
- Cairns, R. A., Harris, I. S., & Mak, T. W. 2011. Regulation of cancer cell metabolism. *Nat. Rev. Cancer*. 11, 85-95.
- Chakrabarti, O., Veeraraghavalu, K., Tergaonkar, V., Liu, Y., Androphy, E. J., Stanley, M. A., & Krishna, S. (2004). Human papillomavirus type 16 E6 amino acid 83 variants enhance E6-mediated MAPK signaling and differentially regulate tumorigenesis by notch signaling and oncogenic Ras. *J. Virol*. 78, 5934-5945.
- Chen, J., Imanaka, N., Chen, J., & Griffin, J. D. 2009. Hypoxia potentiates Notch signaling in breast cancer leading to decreased E-cadherin expression and

- increased cell migration and invasion. *Brit. J. Cancer.* 102, 351-360.
- Chi, J. T., Wang, Z., Nuyten, D. S., Rodriguez, E. H., Schaner, M. E., Salim, A., Wang, Y., Kristensen, G. B., Helland, A., Borresen-Dale, A. L., Giaccia, A., Longaker, M. T., Hastie, T., Yang, G. P., de Vijver, M. J., & Brown, P. O. (2006). Gene expression programs in response to hypoxia: cell type specificity and prognostic significance in human cancers. *PLoS Med.* 3, e47.
- Chiche, J., Ilc, K., Laferrière, J., Trottier, E., Dayan, F., Mazure, N. M., Brahimi-Horn, C., & Pouyssegur, J. 2009. Hypoxia-inducible carbonic anhydrase IX and XII promote tumor cell growth by counteracting acidosis through the regulation of the intracellular pH. *Cancer Res.* 69, 358-368.
- Chilov, D., Camenisch, G., Kvietikova, I., Ziegler, U., Gassmann, M., & Wenger, R. H. 1999. Induction and nuclear translocation of hypoxia-inducible factor-1 (HIF-1): heterodimerization with ARNT is not necessary for nuclear accumulation of HIF-1 $\alpha$ . *J. Cell Sci.* 112, 1203-1212.
- Crow, J. M. 2012. HPV: The global burden. *Nature*, 488, S2-S3.
- Cunningham, S., Jackson, R., & Zehbe, I. 2014. Hypoxia-inducible factor 1 and its role in viral carcinogenesis. *Virology.* 456, 370-383.
- Darnell, J. E. 2002. Transcription factors as targets for cancer therapy. *Nat. Rev. Cancer.* 2, 740-749.
- de Martel, C., Ferlay, J., Franceschi, S., Vignat, J., Bray, F., Forman, D., Plummer, M., 2012. Global burden of cancers attributable to infections in 2008: a review and synthetic analysis. *Lancet Oncol.* 13, 607–615.

- DeBerardinis, R. J., Lum, J. J., Hatzivassiliou, G., & Thompson, C. B. 2008. The biology of cancer: metabolic reprogramming fuels cell growth and proliferation. *Cell Metab.* 7, 11-20.
- DeCarlo, C. A., Escott, N. G., Werner, J., Robinson, K., Lambert, P. F., Law, R. D., & Zehbe, I. 2008. Gene expression analysis of interferon  $\kappa$  in laser capture microdissected cervical epithelium. *Anal. Biochem.* 381, 59-66.
- Depping, R., Steinhoff, A., Schindler, S.G., Freidrich, B., Fagerlund, R., Metzen, E., Hartmann, E., Köhler, M. 2008. Nuclear translocation of hypoxia-inducible factors (HIFs): Involvement of the classical  $\alpha/\beta$  importin pathway. *BBA – Mol. Cell. Res.* 1783, 394–404.
- Doorbar, J., Quint, W., Banks, L., Bravo, I. G., Stoler, M., Broker, T. R., Stanley, M. A. 2012. The biology and life-cycle of human papillomaviruses. *Vaccine.* 30, F55-F70.
- Dhup, S., Kumar Dadhich, R., Ettore Porporato, P., Sonveaux, P. 2012. Multiple biological activities of lactic acid in cancer: influences on tumor growth, angiogenesis and metastasis. *Curr. Pharm. Des.*, 18, 1319-1330.
- Estrella, V., Chen, T., Lloyd, M., Wojtkowiak, J., Cornnell, H. H., Ibrahim-Hashim, A., Bailey, K., Balagurunathan, Y., Rothberg, J. M., Sloane, B.F., Gatenby, R.A., & Gillies, R. J. (2013). Acidity generated by the tumor microenvironment drives local invasion. *Cancer Res.* 73, 1524-1535.
- Gatenby, R. A., Gawlinski, E. T., Gmitro, A. F., Kaylor, B., Gillies, R. J. 2006. Acid-mediated tumor invasion: a multidisciplinary study. *Cancer Res.* 66, 5216-5223.

- Ghittoni, R., Accardi, R., Hasan, U., Gheit, T., Sylla, B., Tommasino, M. 2010. The biological properties of E6 and E7 oncoproteins from human papillomaviruses. *Virus genes*. 40, 1-13.
- Hirschhaeuser, F., Sattler, U. G., Mueller-Klieser, W. 2011. Lactate: a metabolic key player in cancer. *Cancer Res*. 71, 6921 - 6925.
- Hock, A. K., & Vousden, K. H. 2012. Tumor suppression by p53: fall of the triumvirate?. *Cell*. 149, 1183-1185.
- Hsu, P. P., Sabatini, D. M. 2008. Cancer cell metabolism: Warburg and beyond. *Cell*. 134, 703-707.
- Huang, M., Chen, Q., Xiao, J., Yao, T., Bian, L., Liu, C., Lin, Z. 2014. Overexpression of Hypoxia-Inducible Factor-1 $\alpha$  Is a Predictor of Poor Prognosis in Cervical Cancer: A Clinicopathologic Study and a Meta-analysis. *Int. J. of Gynecol. Cancer*, 24, 1054-1064.
- Jackson, R., Togtema, M., Lambert, P. F., & Zehbe, I. 2014. Tumorigenesis Driven by the Human Papillomavirus Type 16 Asian-American E6 Variant in a Three-Dimensional Keratinocyte Model. *PloS One*. 9, e101540.
- Kim, J. W., Tchernyshyov, I., Semenza, G. L., & Dang, C. V. 2006. HIF-1-mediated expression of pyruvate dehydrogenase kinase: a metabolic switch required for cellular adaptation to hypoxia. *Cell Metab*. 3, 177-185.
- Klingelutz, A. J., Foster, S. A., & McDougall, J. K. 1996. Telomerase activation by the E6 gene product of human papillomavirus type 16. *Nature*. 380, 79 – 82.
- Kondoh, H. 2008. Cellular life span and the Warburg effect. *Exp. Cell Res*. 314, 1923-1928.

- Koppenol, W. H., Bounds, P. L., & Dang, C. V. 2011. Otto Warburg's contributions to current concepts of cancer metabolism. *Nat. Rev. Cancer.* 11, 325-337.
- Kroemer, G., & Pouyssegur, J. 2008. Tumor cell metabolism: cancer's Achilles' heel. *Cancer cell.* 13, 472-482.
- Lando, D., Peet, D. J., Gorman, J. J., Whelan, D. A., Whitelaw, M. L., & Bruick, R. K. 2002. FIH-1 is an asparaginyl hydroxylase enzyme that regulates the transcriptional activity of hypoxia-inducible factor. *Gene Dev.* 16, 1466-1471.
- Laughner, E., Taghavi, P., Chiles, K., Mahon, P. C., & Semenza, G. L. 2001. HER2 (neu) signaling increases the rate of hypoxia-inducible factor 1 $\alpha$  (HIF-1 $\alpha$ ) synthesis: novel mechanism for HIF-1-mediated vascular endothelial growth factor expression. *Mol. Cell. Biol.* 21, 3995-4004.
- Liao, D., Johnson, R. S. 2007. Hypoxia: a key regulator of angiogenesis in cancer. *Cancer Metast Rev.* 26, 281-290.
- Lichtig, H., Algrisi, M., Botzer, L. E., Abadi, T., Verbitzky, Y., Jackman, A., Tommasino, M., Zehbe, I., & Sherman, L. 2006. HPV16 E6 natural variants exhibit different activities in functional assays relevant to the carcinogenic potential of E6. *Virology.* 350, 216-227.
- Livak, K. J., & Schmittgen, T. D. 2001. Analysis of Relative Gene Expression Data Using Real-Time Quantitative PCR and the  $2^{-\Delta\Delta CT}$  Method. *Methods.* 25, 402-408.
- Lee, J. W., Bae, S. H., Jeong, J. W., Kim, S. H., Kim, K. W. 2004. Hypoxia-inducible factor (HIF-1)  $\alpha$ : its protein stability and biological functions. *Exp. Mol. Med.* 36, 1-12.

- Levine, A. J., & Puzio-Kuter, A. M. 2010. The control of the metabolic switch in cancers by oncogenes and tumor suppressor genes. *Science*. 330, 1340-1344.
- Lopez-Lazaro, M. 2008. The warburg effect: why and how do cancer cells activate glycolysis in the presence of oxygen?. *Anticancer Agents Med. Chem.* 8, 305-312.
- Lu, J., Tan, M., & Cai, Q. 2014. The Warburg effect in tumor progression: Mitochondrial oxidative metabolism as an anti-metastasis mechanism. *Cancer Lett.* Available online 10 April 2014.
- Mathupala, S. P., Ko, Y. H., & Pedersen, P. L. 2009. Hexokinase-2 bound to mitochondria: cancer's stygian link to the “Warburg Effect” and a pivotal target for effective therapy. *Semin. Cancer. Biol.* 19, 17-24.
- Münger, K., Phelps, W. C., Bubb, V., Howley, P. M., & Schlegel, R. 1989. The E6 and E7 genes of the human papillomavirus type 16 together are necessary and sufficient for transformation of primary human keratinocytes. *J. Virol.* 63, 4417-4421.
- Onder, T. T., Gupta, P. B., Mani, S. A., Yang, J., Lander, E. S., & Weinberg, R. A. 2008. Loss of E-cadherin promotes metastasis via multiple downstream transcriptional pathways. *Cancer Res.* 68, 3645-3654.
- Parks, S. K., Chiche, J., & Pouyssegur, J. 2011. pH control mechanisms of tumor survival and growth. *J. Cell Physiol.* 226, 299-308.
- Patel, D., Huang, S. M., Baglia, L. A., & McCance, D. J. 1999. The E6 protein of human papillomavirus type 16 binds to and inhibits coactivation by CBP and p300. *EMBO J.* 18, 5061-5072.

- Mills, C. N., Joshi, S. S., & Niles, R. M. 2009. Expression and function of hypoxia inducible factor-1 alpha in human melanoma under non-hypoxic conditions. *Mol Cancer*. 8, 49.
- Niccoli, S., Abraham, S., Richard, C., Zehbe, I., 2012. The Asian-American E6 variant protein of human papillomavirus 16 alone is sufficient to promote immortalization, transformation, and migration of primary human foreskin keratinocytes. *J. Virol*. 86, 12384–12396.
- Noch, E., & Khalili, K. 2012. Oncogenic viruses and tumor glucose metabolism: like kids in a candy store. *Mol. Cancer Ther*. 11, 14-23.
- Rathmell, J. C., Fox, C. J., Plas, D. R., Hammerman, P. S., Cinalli, R. M., & Thompson, C. B. 2003. Akt-directed glucose metabolism can prevent Bax conformation change and promote growth factor-independent survival. *Mol. Cell Biol*. 23, 7315-7328.
- Richard, C., Lanner, C., Naryzhny, S. N., Sherman, L., Lee, H., Lambert, P. F., & Zehbe, I. 2010. The immortalizing and transforming ability of two common human papillomavirus 16 E6 variants with different prevalences in cervical cancer. *Oncogene* 29, 3435-3445.
- Semenza, G.L. 2001. HIF-1, O<sub>2</sub>, and the 3 PHDs: how animal cells signal hypoxia to the nucleus. *Cell*. 107, 1–3.
- Semenza, G.L. 2003. Targeting HIF-1 for Cancer Therapy. *Nat. Rev. Cancer* 3, 721–732.
- Semenza, G. L. 2010. HIF-1: upstream and downstream of cancer metabolism. *Current Opin. Genet. Dev*. 20, 51-56.

- Semenza, G.L., 2012. Hypoxia-inducible factors: mediators of cancer progression and targets for cancer therapy. *Trends Pharmacol. Sci.* 33, 207–214.
- Sedman, S. A., Barbosa, M. S., Vass, W. C., Hubbert, N. L., Haas, J. A., Lowy, D. R., Schiller, J. T. 1991. The full-length E6 protein of human papillomavirus type 16 has transforming and trans-activating activities and cooperates with E7 to immortalize keratinocytes in culture. *J. Virol.* 65, 4860-4866.
- Shakya, A., Cooksey, R., Cox, J. E., Wang, V., McClain, D. A., & Tantin, D. 2009. Oct1 loss of function induces a coordinate metabolic shift that opposes tumorigenicity. *Nat. Cell Biol.* 11, 320-327.
- Sonenberg, N., & Gingras, A. C. (1998). The mRNA 5' cap-binding protein eIF4E and control of cell growth. *Curr. Opin. Cell Biol.* 10, 268-275.
- Togtema, M. 2013. Differential response of two common human papillomavirus 16 variants to small interfering RNA. MSc Thesis, Lakehead University, Thunder Bay, Ontario.
- Upadhyay, M., Samal, J., Kandpal, M., Singh, O. V., & Vivekanandan, P. 2013. The Warburg effect: insights from the past decade. *Pharmacol. Ther.* 137, 318-330.
- Vander Heiden, M. G., Cantley, L. C., Thompson, C. B. 2009. Understanding the Warburg effect: the metabolic requirements of cell proliferation. *Science* 324, 1029-1033.
- Walboomers, J. M., Jacobs, M. V., Manos, M. M., Bosch, F. X., Kummer J. A., Shah, K. V., Snijders, P. J., Peto, J., Meijer C., Munoz, N. 1999. Human papillomavirus is a necessary cause of invasive cervical cancer worldwide. *J. Pathol.* 189, 12 – 19.
- Walenta, S., Wetterling, M., Lehrke, M., Schwickert, G., Sundfør, K., Rofstad, E. K., &

- Mueller-Klieser, W. 2000. High lactate levels predict likelihood of metastases, tumor recurrence, and restricted patient survival in human cervical cancers. *Cancer Res.* 60, 916-921.
- Wenger, R.H., Kvietikova, I., Rolfs, A., Gassmann, M., Marti, H.H., 1997. Hypoxia-inducible factor-1 $\alpha$  is regulated at the post mRNA level. *Kidney Int.* 51, 560–563.
- Wilson, W. R., & Hay, M. P. 2011. Targeting hypoxia in cancer therapy. *Nat. Rev. Cancer.* 11, 393-410.
- Wong, C. C. L., Gilkes, D. M., Zhang, H., Chen, J., Wei, H., Chaturvedi, P., Fraley, S. I., Wong, C. M., Khoo, U., Ng, I. O.L., Semenza, G. L. 2011. Hypoxia-inducible factor 1 is a master regulator of breast cancer metastatic niche formation. *P. Natl. Acad. Sci. USA.* 108, 16369-16374.
- Woodman, C. B., Collins, S. I., Young, L. S. 2007. The natural history of cervical HPV infection: unresolved issues. *Nat. Rev. Cancer.* 7, 11-22.
- Wu, C. A., Chao, Y., Shiah, S. G., & Lin, W. W. (2013). Nutrient deprivation induces the Warburg effect through ROS/AMPK-dependent activation of pyruvate dehydrogenase kinase. *BBA – Mol. Cell Research*, 1833, 1147- 1156.
- Xi, L. F., Koutsky, L. A., Hildesheim, A., Galloway, D. A., Wheeler, C. M., Winer, R. L., Ho, J., & Kiviat, N. B. 2007. Risk for high-grade cervical intraepithelial neoplasia associated with variants of human papillomavirus types 16 and 18. *Cancer Epidem. Biomar.* 16, 4-10.
- Yang, M. H., Wu, M. Z., Chiou, S. H., Chen, P. M., Chang, S. Y., Liu, C. J., Teng, S. C., & Wu, K. J. 2008. Direct regulation of TWIST by HIF-1 $\alpha$  promotes metastasis. *Nat. Cell Biol.* 10(3), 295-305.

Zhong, H., De Marzo, A. M., Laughner, E., Lim, M., Hilton, D. A., Zagzag, D., Buechler, P., Isaacs, W. B., Semenza, G. L., Simons, J. W. 1999. Overexpression of hypoxia-inducible factor 1 $\alpha$  is common human cancers and their metastases. *Cancer Res.* 59, 5830-5835

## 7 APPENDIX

		Range 1: 2 to 446 <a href="#">Graphics</a>				
		Score	Expect	Identities	Gaps	Strand
		822 bits(445)	0.0	445/445(100%)	0/445(0%)	Plus/Plus
E6 reference	→ Query	102	CAATGTTTCAGGACCCACAGGCGGACCCAGAAAAGTTACCACAGTTATGCACAGAGCTGC	161		
	→ Sbjct	2	CAATGTTTCAGGACCCACAGGCGGACCCAGAAAAGTTACCACAGTTATGCACASAGCTGC	61		
Sequencing Result	Query	162	AAACAACTATACATGATATAAATTAGAAATGCTGTACTGCAAGCAACAGTTACTGCGAC	221		
	Sbjct	62	AAACAACTATACATGATATAAATTAGAAATGCTGTACTGCAAGCAACAGTTACTGCGAC	121		
	Query	222	GTGAGGTATATGACTTTGCTTTTCGGGATTTATGCATAGTATATAGAGATGGGAATCCAT	281		
	Sbjct	122	GTGAGGTATATGACTTTGCTTTTCGGGATTTATGCATAGTATATAGAGATGGGAATCCAT	181		
	Query	282	ATGCTGTATGTGATAAAATGTTTAAAGTTTTATCTAAAATTAGTGAGTATAGACATTATT	341		
	Sbjct	182	ATGCTGTATGTGATAAAATGTTTAAAGTTTTATCTAAAATTAGTGAGTATAGACATTATT	241		
	Query	342	GTTATAGTTTGTATCGAACAACATTAGAACAGCAATACAACAACCCGTTGCTGATTTGT	401		
	Sbjct	242	GTTATAGTTTGTATCGAACAACATTAGAACAGCAATACAACAACCCGTTGCTGATTTGT	301		
	Query	402	TAATTAGGCTGATTAACCTGTCAAAGCCACTGTGTCTCTGAAGAAAAGCAAAGACATCTGG	461		
	Sbjct	302	TAATTAGGCTGATTAACCTGTCAAAGCCACTGTGTCTCTGAAGAAAAGCAAAGACATCTGG	361		
	Query	462	ACAAAAGCAAAGATTCCATAATATAAGGGGTCGGTGGACCGGTCGATGTATGCTTTGTT	521		
	Sbjct	362	ACAAAAGCAAAGATTCCATAATATAAGGGGTCGGTGGACCGGTCGATGTATGCTTTGTT	421		
	Query	522	GCAGATCATCAAGAACACCTAGAGA	546		
	Sbjct	422	GCAGATCATCAAGAACACCTAGAGA	446		

**Figure A1. Sequence alignment of EPE6 with HPV16 reference sequence.** E6 DNA from Donor One EP transduced keratinocytes was amplified, purified, and sent for Sanger sequencing at the Paleo-DNA Laboratory at Lakehead University. A 100% alignment between the EPE6 DNA sequence and the reference sequence was found confirming EP harboured the reference E6 sequence.

Sequence ID: lcl|184993 Length: 432 Number of Matches: 1

		Score	Expect	Identities	Gaps	Strand	
		730 bits(395)	0.0	405/410(99%)	0/410(0%)	Plus/Plus	
E6 reference	→Query	140	CCACAGT	TATGCCACAGAGCTGCCAAACA	ACTATACATGATATAATATTAGA	ATGTGTGTAC	199
	→Sbjct	14	CCACAGT	TATGCCACAGAGCTGCCAAACA	ACTATACATGATATAATATTAGA	ATGTGTGTAC	73
Sequencing Result	→Query	200	TGCAAGCAACAGTTACTGCCACG	TGAGGTATATGACTTTGCTTTTC	GGGATTTATGCATA		259
	→Sbjct	74	TGCAAGCAACAGTTACTGCCACG	TGAGGTATATGACTTTGCTTTTC	GGGATTTATGCATA		133
E6 reference	→Query	260	GTATAEAGAGATGGCAATCCAT	ATCTGAT	GTGATAAATGTTTAAAGTTT	TATTCTAAA	319
	→Sbjct	134	GTATAEAGAGATGGCAATCCAT	ATCTGAT	GTGATAAATGTTTAAAGTTT	TATTCTAAA	193
Sequencing Result	→Query	320	ATTAGTGAGTATAACATTAAT	TGTTAAGTTT	GTATGGAACAACATTAGAAC	CAGCAATAC	379
	→Sbjct	194	ATTAGTGAGTATAACATTAAT	TGTTAAGTTT	GTATGGAACAACATTAGAAC	CAGCAATAC	253
E6 reference	→Query	380	AACAAACCGTGTGTGATTTG	TAAATAGGTTTAACTGTCAA	AAGCCACTGTGTCCCT		439
	→Sbjct	254	AACAAACCGTGTGTGATTTG	TAAATAGGTTTAACTGTCAA	AAGCCACTGTGTCCCT		313
Sequencing Result	→Query	440	GAAGAAAAGCAAAGACATCT	GACAAAAGCAAAGATTCCAT	AATATAAGGGTCCGGTGG		499
	→Sbjct	314	GAAGAAAAGCAAAGACATCT	GACAAAAGCAAAGATTCCAT	AATATAAGGGTCCGGTGG		373
E6 reference	→Query	500	ACCGGTCGATGTATGTCTT	GTGTCAGATCATCAAGAAC	ACGTAGAGAAAC		549
	→Sbjct	374	ACCGGTCGATGTATGTCTT	GTGTCAGATCATCAAGAAC	ACGTAGAGAAAC		423

**Figure A2. Sequence alignment of AAE6 with HPV16 reference sequence.** E6 DNA from Donor One AA transduced keratinocytes was amplified, purified, and sent for Sanger sequencing at the Paleo-DNA Laboratory at Lakehead University. The expected 5 highlighted SNPs were found between the AAE6 DNA sequence and the reference sequence was found confirming AA harboured the Asian-American variant. The 6<sup>th</sup> expected SNP couldn't be confirmed due to it being located within the reverse primer sequence and outside the range of the forward primer